Trends in Building Materials Research

Part 1

Edited by
Jianjun Zheng, Xiuli Du, Weiming Yan,
Yue Li and Jianwei Zhang

TRANS TECH PUBLICATIONS

Trends in Building Materials Research

Edited by
Jianjun Zheng
Xiuli Du
Weiming Yan
Yue Li
Jianwei Zhang

Trends in Building Materials Research

Selected, peer reviewed papers from the
2nd International Conference on
Structures and Building Materials
(ICSBM 2012),
March 9-11, 2012, Hangzhou, China

Edited by

**Jianjun Zheng, Xiuli Du, Weiming Yan,
Yue Li and Jianwei Zhang**

TTP

Trans Tech Publications Ltd
Kreuzstrasse 10
CH-8635 Durnten-Zurich
Switzerland
http://www.ttp.net

Volumes 450-451 of
Advanced Materials Research *2-vol.-set*
ISSN 1022-6680

Full text available online at *http://www.scientific.net*

***Distributed** worldwide by*

Trans Tech Publications Ltd
Kreuzstrasse 10
CH-8635 Durnten-Zurich
Switzerland

Fax: +41 (44) 922 10 33
e-mail: sales@ttp.net

and in the Americas by

Trans Tech Publications Inc.
PO Box 699, May Street
Enfield, NH 03748
USA

Phone: +1 (603) 632-7377
Fax: +1 (603) 632-5611
e-mail: sales-usa@ttp.net

Preface

The Second International Conference on Structures and Building Materials (ICSBM 2012) was held from March 9 to March 11, 2012, in Hangzhou, China. The conference goal was to highlight case studies and research on new and innovative ways to achieve sustainable construction practices through use of novel building materials and technologies.

We would like to extend our thanks to the technical committees for bringing their extensive multi-disciplinary experience to the rigorous peer reviews that they have conducted, as well as all the hard work they have put into the build-up to this conference to help make it a success with the important input, of course, from you the delegates. Additionally, we would also like to extend our thanks to all the authors, session chairs, session moderators, and delegates for their contribution.

Finally we would like to extend an invitation to you, the reader, to think about submitting an abstract to the next international conference on structures and building materials to further the study and promulgation of this important topic.

The Organizing Committee of ICSBM 2012

Sponsored by

The College of Architecture and Civil Engineering,

Beijing University of Technology

School of Civil Engineering and Architecture,

Zhejiang University of Technology

Conference Organization

Co-Chairmen

Prof. Xiuli Du, Beijing University of Technology, China

Prof. Jianjun Zheng, Zhejiang University of Technology, China

Technical and Organizing Committee

Prof. Xiuli Du, Beijing University of Technology, China

Prof. Yong Huang, Guizhou University, China

Prof. Chaohe Chen, Hainan University, China

Prof. Weiliang Jin, Zhejiang University, China

Prof. Jianguo Nie,Tsing Hua University, China

Prof. Bo Wu, South China University of Technology, China

Prof. Shilang Xu, Zhejiang University, China

Prof. Jianjun Zheng, Zhejiang University of Technology

Prof. Boyang Ding, Zhejiang University of Technology

Prof. Minyun Hu, Zhejiang University of Technology

Prof. Zhiyong Dong, Zhejiang University of Technology

Prof. Xinjun Zhang, Zhejiang University of Technology

Prof. Fuying Liu, Zhejiang University of Technology

Academician Prof. Wei Sun, Southeast University, China

Prof. Ailin Zhang, Beijing University of Technology, China

Prof. Weiming Yan, Beijing University of Technology, China

Prof. Bin Xu, Hunan Univercity, China

Prof. Feng Fan, Harbin Institute of Technology, China

Prof. Lijuan Li, Guangdong University of Technology

Prof. Yiqiang Xiang, Zhejiang University, China

Prof. Peiyu Yan, Tsinghua University, China

Prof. Feng Liu, Guangdong University of Technology

Prof. Jun Deng, Guangdong University of Technology

Prof. Jianxun Ma, Xi'an Jiaotong University, China

Prof. Jichao Zhang, Guangzhou University, China

Prof. Linhai Han, Tsinghua University, China

Prof. Wenguang Liu, Shanghai University, China

Prof. Yanpeng Zhu, Lanzhou University of Technology, China

Prof. Yun Zhou, Guangzhou University, China

Prof. Zhengliang Li, Chongqing University, China

Prof. Zhihua Chen, Tianjin University, China

Prof. Guangfan Li, Hainan University, China

Prof. Jiping Hao, Xi'AN Univ. of Architecture and Tech., China

Prof. Jihong Ye,Southeast University, China

Prof. Zixiong Guo, Hua Qiao University, China

Prof. Xuejun Zhou, Shandong Jianzhu University, China

Dr. Tianjian Ji, The University of Manchester, UK

Prof. Tamon UEDA, Hokkaido University, Japan

Prof. Tan Kiang Hwee, National University of Singapore

Prof. Tim Ibell, University of Bath, UK

Prof. Zong Woo Geem, iGlobal University, USA

Prof. Zhi-Shen Wu, Ibaraki University, Japan

Local Organizing Committee

Dr. Jianwei Zhang, Beijing University of Technology

Dr. Sifa Xu, Zhejiang University of Technology

Dr. Mark Fong, Hong Kong Industrial Technology Research Centre

Table of Contents

Chapter 2: Advanced Construction Materials

Chapter 3: Green Building Materials

Chapter 4: Architectural Design and its Theory

Chapter 5: Urban Planning and Design

Chapter 6: Landscape Planning and Design

Chapter 7: Building Energy Saving Technology

Chapter 8: Ecological Architecture

CHAPTER 1:

Traditional Construction Materials

Advanced Materials Research Vols. 450-451 (2012) pp 3-7

doi:10.4028/www.scientific.net/AMR.450-451.3

Evolution of Capillary Porous Structure in Steam Curing Concrete with Mineral Admixtures

BA Mingfang[1, a], QIAN Chunxiang[2,b]

[1]Faculty of Architectural Civil Engineering and Environment, Ningbo University, Ningbo, 315211, China

[2]School of Materials Science and Engineering, Southeast University, Nanjing, 211189, China

[a]bamingfang@nbu.edu.cn, [b]cxqian1966@126.com

Keywords: Capillary pores; Evolution; Precast concrete; Steam curing duration

Abstract. The capillary porous structures of the pre-cast concrete with different initial steam-curing duration were analyzed with MIP techniques. Then the hydration degree of cement, fly ash and slag in pre-cast concrete versus time were obtained respectively by combing the hydrochlorides and EDTA selecting dissolution methods, based on which the corresponding evolution of capillary porosity was determined. The comparison between calculated results and experimental capillary porosity showed that the proposed evolution model of capillary porosity could be adopted to reveal the developing trend of capillary porosity of pre-cast concrete with fly ash and slag under certain curing conditions.

Introduction

Concrete durability depends largely on its complex microstructures and the level of possibility of harmful gases or ions' entry into concrete [1]. The capillary pore structures was considered as major transport channels inside concrete [2,3]. The hydration kinetics of cement has been modeled by a lot of literatures [4-7] while the corresponding one in concrete with pozzolanic admixtures was arising wide attention in recent literatures [8]. It is well known that the dynamic hydration kinetics of composite cemented materials in concrete determined the capillary pore structures.

Few of research reports included the effects of temperature or different curing condition on the evolution of capillary pore structures of precast concrete with several mineral admixtures [9]. This paper just provided a chemical analysis method to determine the development of hydration degree of single cement, fly ash and slag in concrete with certain curing condition, respectively. Then evolution of capillary pore in concrete with certain curing condition could be calculated base on the hydration models proposed in literatures. Moreover the calculated capillary porosity of the pre-cast concrete was compared with corresponding experimental results by MIP.

Experimental

The mixtures were made with Chinese normal Portland cement P.I52.5. The used granulated blast furnace slag and fly ash was name S95 and I grade according ASTM C618.The corresponding chemical composition were shown in Table 1.

Table 1 Chemical components and physical properties for cementicious materials

Type of binder	Chemical compostion /%										Density /kg/m^3
	Loss	SiO_2	Al_2O_3	Fe_2O_3	CaO	MgO	SO_3	K_2O	Na_2O	Total	
P·I 52.5	2.29	19.49	4.08	4.03	64.59	1.97	2.33	0.37	0.07	99.22	3145
Fly-ash	3.21	56.02	28.00	6.20	3.60	1.21	0.61	0.89	0.23	99.97	2550
Slag	0.03	34.35	2.35	15.20	35.38	8.54	0.12	0.32	0.63	96.92	2896

Natural sand with 2.9 fineness modulus and crushed granite rocks with 5~25 mm particles were used as fine and coarse aggregates. And table 2 showed the corresponding mixture proportions.

Table 2 Concrete proportions / kg/m^3

No	Cement	Flyash	Slag	Crushed stone (10-20mm）	Crushed stone （5-10mm）	Sand	Water	Superplasticizer
FS	322	83	55	736	397	694	140	3.22

Four groups of specimen with dimension of 70mm×70mm×300mm was prepared in terms of Table 2 and three groups of them was steam cured at 50°C for 5h, 14h and 24h respectively and one group was cured in standard condition as reference sample. Then all specimens were placed in limewater at 20±1°C for 14d and after then they were moved out and put in room at 20±2°C with 70±5% until 90d age. Finally the capillary pore structures of each specimen were analyzed by MIP methods.

Evolution model of capillary porosity of concrete

Concrete pores consist of capillary and gel pores and capillary pores had great effects on transmission performance of concrete. Thus according to hydration theory of T.C Powers[10] and calculating formula of capillary pore proposed by Bentz [6], the developing equation of capillary pores with time can be expressed as

$$\phi'_{cap}(t) = [\frac{w_0/\rho_w - (V_{\exp,c} + V_{shr}) \cdot m_c/\rho_c \cdot \alpha_c(t)}{m_c/\rho_c + w_0/\rho_w}] \cdot A \quad (1)$$

Where ρ_c=density of cement, kg/m^3 and w/c= water to cement ratio of paste. $V_{\exp.c}$ is the volume difference between hydrates and unhydrates and volume shrinkage of per-volume cement. A — The volume fraction of paste in per-cubic concrete. For concrete with fly ash and slag, the evolution equation of capillary pores in concrete can be expressed as

$$\phi_{cap}(t) = [\frac{w_0/\rho_w - (V_{\exp,c} + V_{shr,c}) \cdot m_c/\rho_c \cdot \alpha_c(t) - V_{\exp,f} \cdot m_f \cdot \alpha_f(t) - V_{\exp,s} m_s \cdot \alpha_s(t)}{(m_c/\rho_c) + (m_f/\rho_f) + (m_s/\rho_s) + (w_0/\rho_w)}] \cdot A \quad (2)$$

Where ρ_f and ρ_s is density of fly ash and slag respectively, kg/m^3. ρ_w is the density of water and w_0 is the water content in per-cubic concrete, kg/m^3; $V_{\exp \cdot c}$, $V_{shr \cdot c}$, $V_{\exp \cdot f}$ and $V_{\exp \cdot s}$ is the volume difference between hydration products and reactants in per-mass cement, fly ash and slag respectively,m^3/kg, which can be deduced in literature[6,11].

Experimental capillary pore structures

Capillary pore of concrete has two parameter named threshold pore (D_t) and critical pore (D_c), which are related with concrete durability. Fig.1 illustrated the effects of steam curing duration on capillary porous structures.

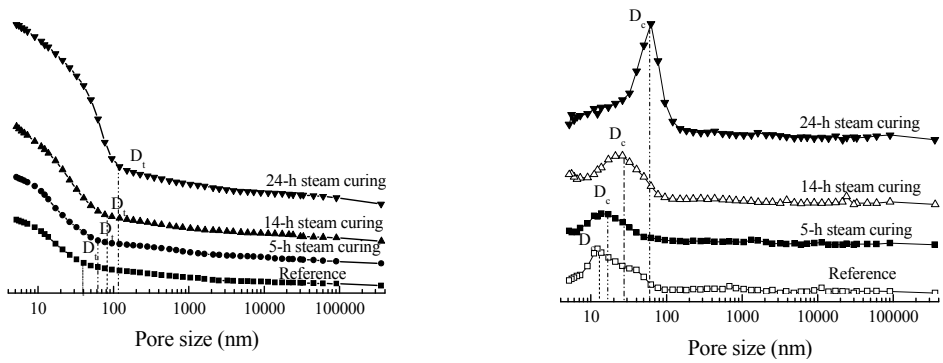

(a) Cumulative porosity curve (b) Pore distribution curve

Fig.1 Capillary pore structures of sample with different steam curing time

It was seen from Fig.1 that with the increase of initial steam-curing duration D_t and D_c correspondingly increased.
Fig.2 showed the relation between above two pore parameters and the initial steam-curing duration. It could be seen from Fig.2 that 14-horu initial steam-curing time, the difference between D_t and D_c increased with increased duration. This indicated that the capillary pores were coarsened by the longer initial steam-curing porosity and the preferable initial steam-curing duration is 14 hour for the concrete sample.

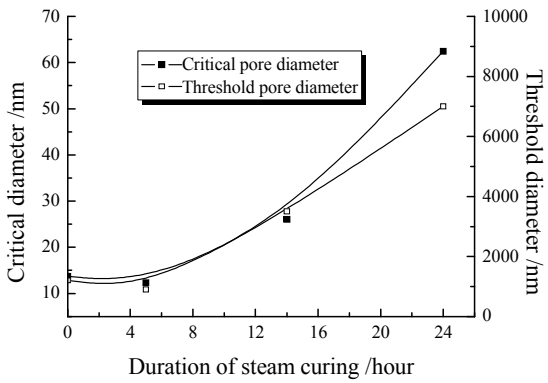

Fig.2 Relationship between pore parameters and initial steam curing time

The capillary porous structures evolution of concrete with 14-hour steam curing duration had been measured by MIP analysis and Fig.3 illustrated the porosity variation with hydration ages. It could be seen that the capillary porosity of sample decreased quickly at early ages and began to be about 4%-5% by the age of 28 days.

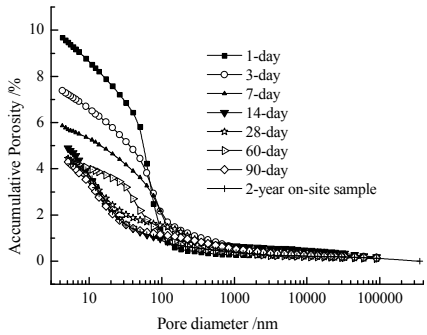

Fig.3 Cumulative capillary porosity with hydration time

Then according to the determined calculating equation of capillary porosity in concrete, capillary porosity of experimental concrete sample could deduced as

$$\phi_{cap} = 10.31\exp(-t/4.27) + 4.08 \quad (3)$$

The distribution of capillary pores was shown in Fig.4. It could be seen that the critical pore diameter was between 80-100nm at the early ages while at the later ages the critical capillary pore diameter decreased to 10-30nm or so.

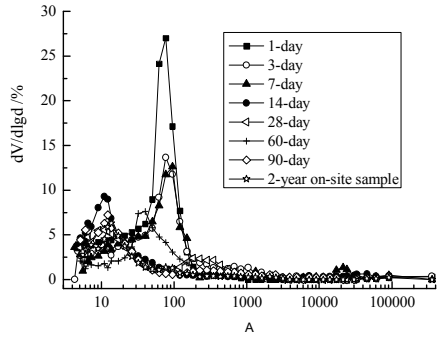

Fig.4 Capillary porosity and distribution of concrete with ages

Comparison of experimental and calculated capillary porosity

The capillary porosity of sample concrete was calculated according to the determined dynamic parameter of fly ash, slag and cement in other parts of this research work. The comparison between experimental and calculated results was illustrated in Fig.5. It could be seen that the changing trend of calculated capillary porosity was very consistent with that of experimental ones. This indicated that the proposed calculating equation of capillary porosity could be adopted to analyze the changing trend of pre-cast concrete segment with certain curing condition. It could also be seen that the capillary porosity was changing around 4.08% after 60-day hydration age without considering other kinds of destruction on concrete.

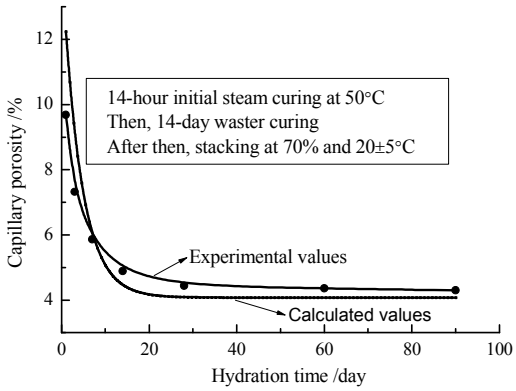

Fig.5 Experimental and calculated capillary porosity of segment concrete with different ages

Conclusions

(1) The capillary pores were coarsened by the longer initial steam-curing porosity and there exists a effective initial steam curing duration. For the studied concrete sample, its preferable initial steam-curing duration is 14 hours.

(2) According to hydration mechanism of cemented materials, the dynamic model of capillary porosity in concrete with certain curing condition could be determined. And the comparison between calculated and experimental capillary porosity showed that the determined dynamic model of capillary porosity could be used to predict the developing trend of capillary porosity in concrete under certain cuing condition.

(3) It could also be concluded that the critical pore diameter of concrete took on a decreasing trend with the prolonged hydration ages.

Acknowledgements

This work was supported by the Zhejiang Open Foundation of the Most Important Subjects and also sponsored by K.C Wong Magna Fund in Ningbo University.

References

[1] S.Y. Huang, J.F. Jiang, N.Y. Yang etc. Modern Concrete Technology, Science and Technology of Shanxi Press, Xian, 2002. (In Chinese)

[2] C.Y. Hu, X.M. Yuan, X.S. Gao. Structure and Performance of Cement Concrete[M]. Chinese Construction Industry Press, Beijing, 1984. (In Chinese)

[3] I. Jawed, J. Skalny, Hydration of tricalcium silicate in the presence of fly ash, Proceedings of Symposium N on Effects of Fly Ash Incorporation in Cement and Concrete, Materials Research Society, Boston, 16– 18 November 1981, pp. 60–70.

[4] F. Lin, C. Meyer. Cement and Concrete Research, 2009, 39:255-265.

[5] P. Navi, C. Pignat. Advanced Cement Based Material 4 (2) (1996) 58–67.

[6] D.P. Bentz. Journal of American Ceramic Society 80 (1):(1997) 3–21.

[7] M. Cervera, R. Faria, J. Oliver, T. Prato. Computers and Structures, 2002, 80:(18–19):1511–1521.

[8] A.K. Schindler, K.J. Folliard. ACI Materials Journal, 2005, 102 (1): 24–33.

[9] H.H. Patel, C.H. Bland, A.B. Poole. Cement and Concrete Research, 1995, 25(3):485-490.

[10] T.C. Powers, T.L. Brownyard. Studies of the physical properties of hardened portland cement paste, Bulletin, vol. 22, Research Laboratories of the Portland Cement Association, Chicago, 1948.

[11]Papadakis V G. Cement and Concrete Research, 1999, 29 (11): 1727–1736.

Advanced Materials Research Vols. 450-451 (2012) pp 8-13

doi:10.4028/www.scientific.net/AMR.450-451.8

Development of cementitious materials with high resistance to sulfate attack by a combination of emulsified asphalt and fly ash

LONG Guangcheng [1, a], LI Zhe[1,b], MA Kunlin[1,c] and XIE Youjun[1]

[1] School of Civil Engineering of Central South University, Changsha City 410075, P.R. China

[a]longguangcheng@csu.edu.cn, [b]532237919@qq.com, [c]mark_mkl@126.com

Keywords: cementitious materials; sulfate attack; emulsified asphalt; fly ash

Abstract. Attack of sulfate crystallization and chemical interaction between sulfate and hydration product is one of the most important factors responsible for degradation of cementitious materials. This study investigates the effects of emulsified asphalt and fly ash as well as their combination on resistance of mortar to physicochemical attack of sulfate in order to develop high performance cementitious materials with high resistance to sulfate attack. The partly-submerged experiment with 5% Na_2SO_4 solution is designed to simulate physicochemical attack of sulfate salt on sample. Results indicate that, compared with fly ash, addition of emulsified asphalt is more effective in improving the resistance of mortar sample to physical crystallization role and chemical attack of sulfate. Moreover, a combination of fly ash and emulsified asphalt can further enhance the resistance of cementitious materials to physicochemical attack of sulfate, which results from the improvement of microstructure, reduction of CH product and increase of ductility of sample.

Introduction

It is well known that ambient sulfate attack is one of the main factors resulted in deterioration of served concrete structure and therefore sulfate attack on cement concretes has been greatly documented over the last several decades [1-9]. Sulfate attack to cementitious materials is a complex process that involves the movement of sulfate ions through the pores by different transportation mechanisms. Once sulfate ion enters into cementitious materials the physicochemical process such as physical crystallization role of sulfate and chemical action of aggressive ion (SO_4^{2-}) with hydration products will occur[1,3,5,9], which will cause severe degradation of concrete. Different methods, such as full immersion test, dry-wet cycle test and half immersion test, were developed to simulate sulfate attack process on cementitious materials and thus to evaluate resistance of cementitious materials to sulfate attack[10-11]. Based on above analysis, in this paper the half-immersion test method is used to simulate the physicochemical attack of sulfate on cementitious materials in practice, such as the crystallization role and aggressive chemical action between SO_4^{2-} and cement hydration products. Some new measurements including combination of emulsified asphalt and mineral admixture (fly ash) are developed to improve the resistance of cementitious materials to severe sulfate attack.

Experimental details

Raw materials. Portland Cement named as P.O 42.5 from Nanfang Cement Plant located in Ningxiang City of Hunan Province of China was used, complying with the Chinese National Standard GB 175-1999. F class fly ash (denoted as FA) with a specific area of 450 m^2/kg used is from Xiangtan Power Plant. The physical properties and chemical compositions of cement and fly ash are given in Table 1. River sand with a modulus of 2.62 was used as aggregate of mortar. Sodium sulfate chemical agent and tap water are used to prepare 5% Na_2SO_4 solution. Emulsified asphalt (EA) is provided by Guangdong Nanyue Logistics Group and its physical and chemical properties are shown in Table 2. One commercial admixtures, alkali metal silicate liquid (WA), is also used. The mixing proportion of sample is listed in Table 3.

Table 1 Chemical oxide composition of cement and fly ash / % by weight

	SiO_2	Al_2O_3	Fe_2O_3	CaO	MgO	SO_3
Cement (C)	21.3	5.8	3.9	59.7	3.4	2.3
Fly ash(FA)	54.0	25.1	9.3	3.7	1.2	0.3

Table 2 Physical properties of emulsified asphalt

Viscosity at 25℃	Residual /% by weight	Penetration depth at 25℃	Softening point
6	60.5	68	56 ℃

Table 3 Mixing proportions of mortar samples / by weight

Serials	Composition of raw materials				
	cement	Fly ash（FA）	admixture	sand	Water/binder
1#(control sample)	1.0	0	0	3.0	0.5
2#	0.75	0.25	0	3.0	0.5
3#	1.0	0	0.03（EA）	3.0	0.5
4#	1.0	0	0.06（EA）	3.0	0.5
5#	1.0	0	0.02（WA）	3.0	0.5
6#	0.75	0.25	0.03（EA）	3.0	0.5

Note: water/binder expresses water to total of cement and fly ash ratio by weight.

Test methods. According to the mixing proportions of different mixtures shown in Table 3, the samples were mixed in mortar mixer and then the mortar sample with a size of 40mm× 40mm × 160mm was cast. The sample was cured in water with 20±2℃ after demoulded at 1 day age. All samples at 14-day age were partly submerged into 5%Na_2SO_4 solution, i.e. two third of height of sample was exposed atmosphere and one third of height was submerged into solution. This experiment was carried out in controlling environment room with (20±3)℃ temperature and (60±5)%RH. Every three days the concentration of solution and its amount were checked and added in order to keep a similar solution condition. From the beginning of this experiment, the mass of all samples was recorded at each interval time. The crystal on surface of sample was not removed when the mass of sample was weighed. The flexural and compressive strength of sample was tested when the experiment finished at one year. And then some typical samples were chosen to analyze corresponding microstructure by SEM test.

Results and discussions

The mass change of sample with immersion age. Fig.1 gives the results of mass change of samples with different compositions. One can find that, from the results shown in Fig.1, the mass for each sample increases with the increasing immersion time. However, the change of mass of samples with the partly submerged age differs from each other. When the partly submerged age is more than 90 days the mass for most samples increases rapidly with the extended immersion age. In the case of sample only with Portland cement, it shows a maximum incremental in mass. However, the mass increment of sample with EA is less than that of sample with FA. The most worthwhile is that the mass of sample with EA and FA almost keeps constant within the whole experimental period. Obviously, the change of mass of sample mainly results from the substances exchange between solution and sample and the loss of water of sample caused by evaporation role during partly submerged experiment period. The increase of mass of sample with immersion age indicates that much substances of solution gradually enter into sample through capillary pore. The more the

substance enters into sample from solution, the more the mass of sample increases. The difference in pore structure of different samples is responsible for the difference in change of mass with partly submerged age.

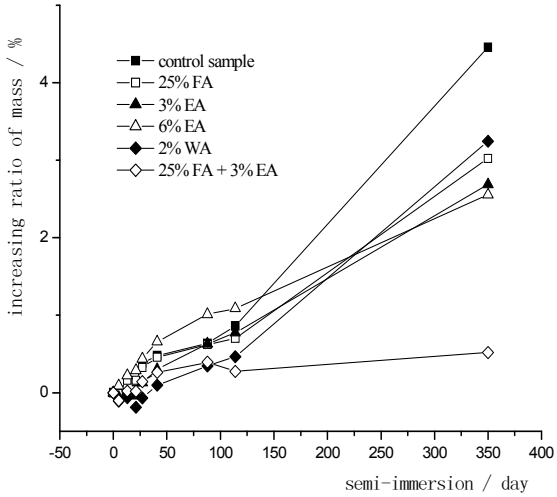

Fig.1 Effects of compositions on mass change of sample with partly submerged age;

Appearances of samples after one year by partly submerged treatment. For the sake of further understanding directly the sulfate attack on mortars with different compositions, the typical appearances of different samples were taken picture and shown in Fig.2 when the one year half-immersion test finished.

From the pictures shown in Fig.2, one can see that the appearance of samples differs greatly from each other after one year partly submerged experiment. In the case of control sample (serial 1#), serious crack is observed. At the same time, much crack can also be found in samples incorporating WA admixture (serial 5#). For other samples such as serial 2#, 3#, 4# and 6#, there are only some small flaws and even no obvious crack are observed on their surface, especially for serial 6# sample keeps in good condition. Crack mainly results from the physical crystallization of sulfate and the generation of expansive product between sulfate and cement hydration product of sample. The more the crystal of sulfate and expansive product exists in sample, the more serious the sample cracks. It can follow that the sample with EA and FA has better resistance to sulfate attack of physical crystallization and aggressive chemical action with cement hydration product.

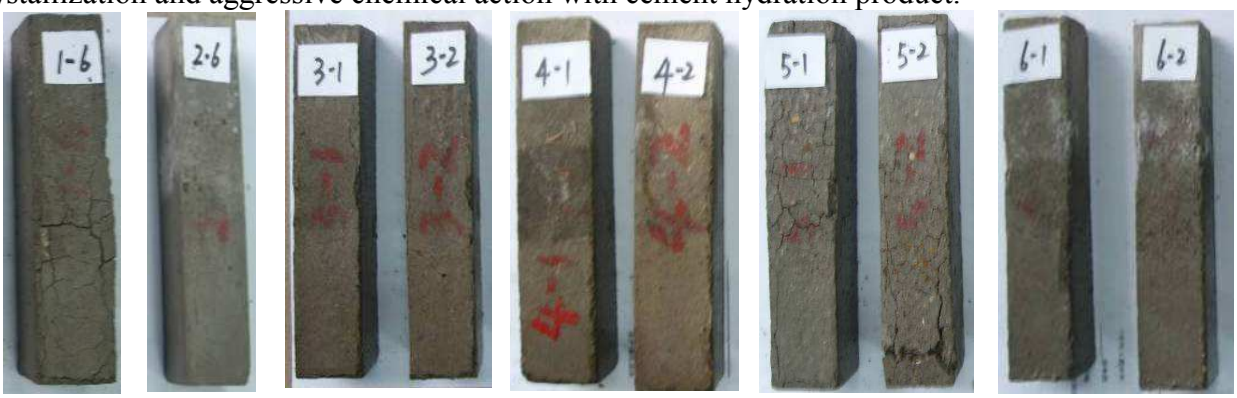

(a) Serial 1# (b) Serial 2# （c）serial 3# （d）serial 4# （e）serial 5# (f) serial 6#

Fig.2 Pictures of samples appearance after 1 year partly submerged experiment

Strength reduction of different samples after one year by partly submerged treatment. Flexural and compressive test of different samples were carried out according to standard method after finished the half-immersion experiment. The corresponding results are listed in Fig.3.

The results given in Fig.3 indicate that the sample with fly ash or emulsified asphalt has higher flexural strength and the flexural to compressive strength ratio compared with that of control sample. And it shows that emulsified asphalt is more effective in improving the resistance of mortar to sulfate

attack. Meanwhile, a combination of fly ash and emulsified asphalt can further improve the strength of sample subjected to 5%Na_2SO_4 partly submerged treatment for one year. The result of strength of sample is consistent with the appearance change of samples as seen in Fig.2

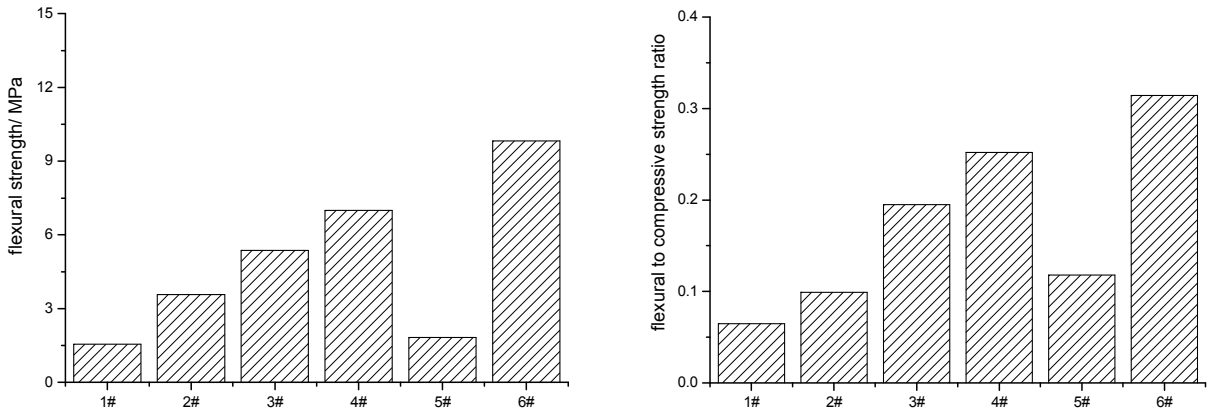

(a) flexural strength (b) flexural to compressive strength ratio

Fig. 3 Strength of different samples suffering 5% Na_2SO_4 partly submerged treatment one year

Mechanisms. After finished strength test of sample, some typical samples were chosen to carry out microstructural analysis by scanning electronic microscope test(SEM) in order to deep understand corresponding mechanisms. The SEM pictures are shown in Fig.4. It can be seen that from the pictures shown in Fig.4, in the case of control sample, there are much cracks observed in the interior and much club-shaped secondary sulfate product existed. For the sample with fly ash(see Fig.4b), one can see some fly ash particle and numerous hydration products in interior of sample with a magnification of 500. And several cracks can be found around fly ash particle in sample with a magnification of 5,000. Fly ash particle seems become an obstacle of crack propagation. It is surprising to find lots of ettringite crystal in the SEM picture of sample with 2% WA and the ettringite with regular shape forms into a porous meshwork structure. This indicates that addition of WA admixture accelerates the formation of expansive secondary sulfate products, which results in a serious damage of sample. As to the sample incorporating emulsified asphalt and fly ash with a magnification of 1000, we can see much cluster flocculent substance and plenty of continual interwoven substance under a magnification of 10,000, which is the polymer structure of emulsified asphalt. And also several small crystal substances can be observed, which were enveloped by the continual network of film structure of emulsified asphalt.

From above microstructure analysis by SEM, it can be followed that under 5% Na_2SO_4 solution partly submerged condition, not only the physical crystallization role of sulfate but also the secondary sulfate product formation such as ettringite are both responsible for the deterioration of sample. However, samples with different compositions have remarkable different resistance to such physicochemical attack of sulfate due to the disparity in the microstructure of sample, crystallization rate and aggressive secondary sulfate product formation. Addition of fly ash can reduce the amount of portlandite (CH) which is prone to interact with SO_4^{2-} to form ettringite and also the rigid fly ash particles can prevent crack from propagation. Emulsified asphalt, as a polymer, can reduce permeability of sample and improve ductility, which will benefit for resistance of cementitious materials to physicochemical attack of sulfate. A combination of fly ash and emulsified asphalt can play a synergetic effect in improving the performance of cementitious materials subjected to sulfate attack.

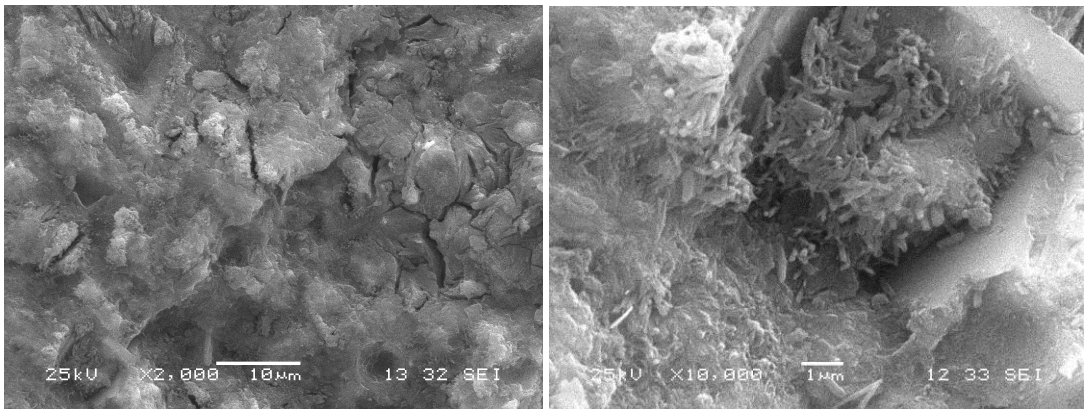

（a）control sample (serial 1#)

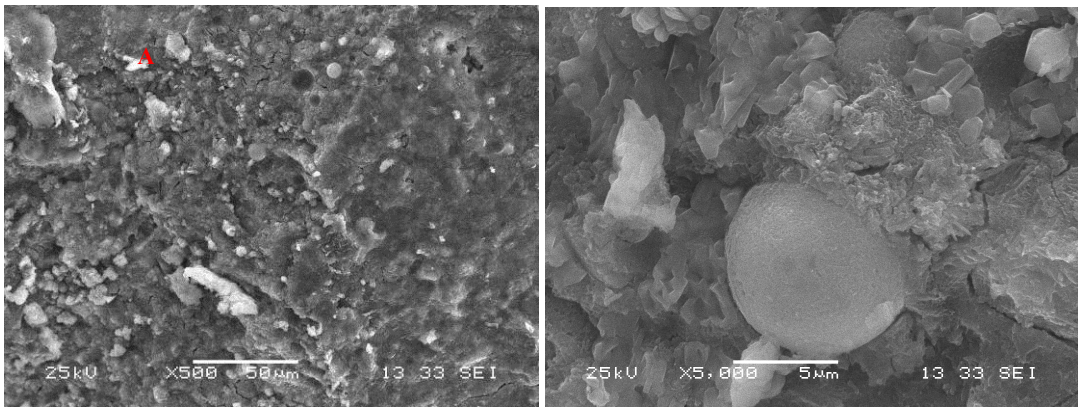

(b) sample with 25% F A (serial 2#)

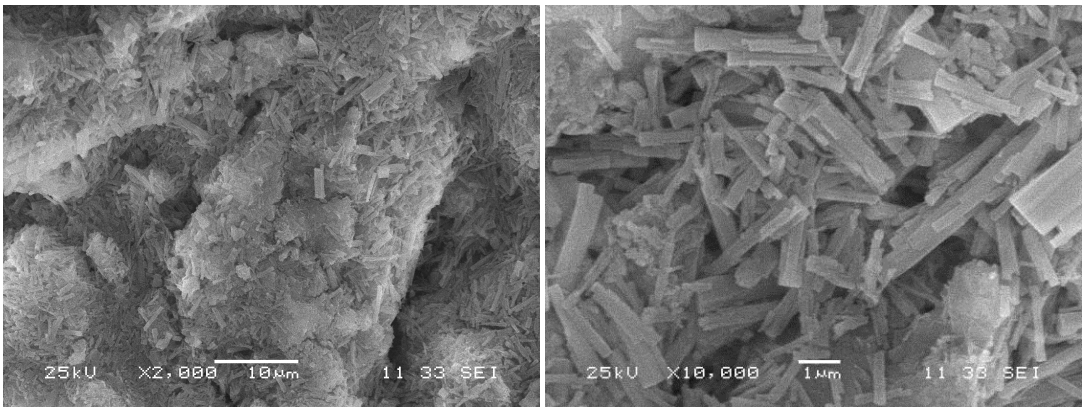

(c) sample with 2% WA (serial 5#)

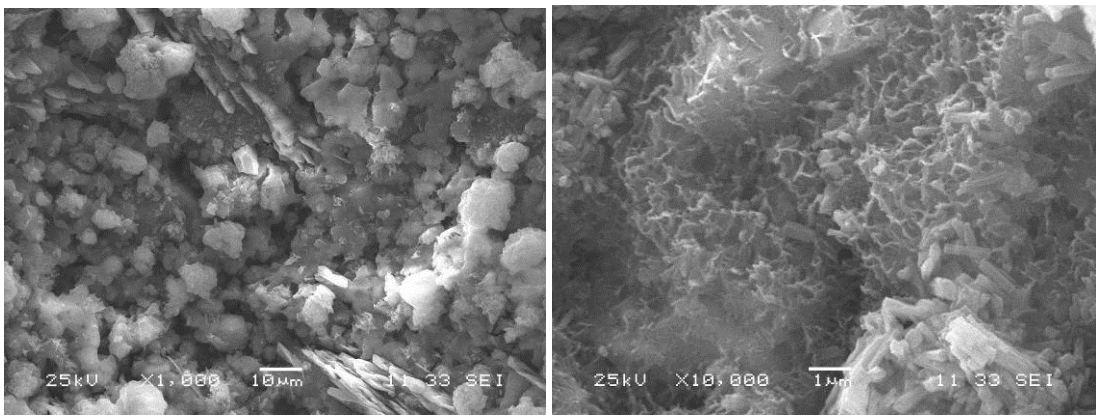

(d) sample with 6% emulsified asphalt (serial 6#)

Fig.4 SEM pictures of samples suffering to 5% Na_2SO_4 partly submerged treatment one year

Conclusions

Not only the physical crystallization role of sulfate but also the secondary sulfate product formations such as ettringite are both responsible for the deterioration of cemenitious materials subject to 5% Na_2SO_4 solution partly submerged treatment. The resistance of cementitious materials to such physicochemical attack of sulfate is remarkably influenced by its compositions. Compared with fly ash, addition of emulsified asphalt is more effective in improving the resistance of mortar sample to physical crystallization and chemical attack of sulfate. Moreover, mortar incorporating a combination of fly ash and emulsified asphalt shows further improvement of resistance to sulfate physicochemical attack, which results from the reduction of CH, improvement of microstructure and increase of ductility of sample.

Acknowledgements

This work was financially supported by National Natural Science Foundation (51108463) and the Leading-edge Research Program of Central South University (2010QZZD018)

References

[1] P.K.Metha. Cement and Concrete Research，Vol. 13, No. 3, 1983, pp401-406

[2] G Odler. Journal of the American Ceramic Society, Vol. 71, No. 11, 1988, pp1015-1020

[3] Haynes H, Neill R, Metha P K. Concrete International, Vol. 16, No. 1, 1996, pp63-68

[4] M Santhanam, M D Cohen, J Oleek. Cement and Concrete Research, Vol. 31, No. 6, 2001, pp 845-851

[5] W Brown. cement & concrete composites, Vol. 24, No. 3, 2002, pp301-303

[6] Omar S.Baghabra Al-Amoudi. Cement and Concrete Composites, Vol. 24, No. 3, 2002, pp 305-316

[7] SHI Minxia, XIE Youjun, LIU Baoju. Journal of Building Materials, Vol. 6, No. 4, 2003, pp350-356*(in Chinese*)

[8] M Santhanam, M D. Cohen. Cement and Concrete Research, Vol. 33, No. 2, 2003, pp 341-346

[9] E.A. Nevill.. Cement and Concrete Research, Vol. 34, No. 8, 2004, pp 1275-1296

[10] Ma Kunlin, *Mechanism and Evaluation Method of Salt Crystallization Attack on Concrete[D]*, Ph-D thesis, Central South University, 2009.6 *(in Chinese)*

[11] LIU Zanqun. *Study of the fundamental of Sulfate Attack on Cementitious Materials[D]*. Changsha: Ph-D thesis, Central South University, 2010.5 *(in Chinese)*

Advanced Materials Research Vols. 450-451 (2012) pp 14-20

doi:10.4028/www.scientific.net/AMR.450-451.14

Research on the effect of concentration and type of de-icing salt on concrete salt-scaling

Qiang Li [1, a], Zhi-yun Zhou [1, b]

[1] School of Environment and Architecture, University of Shanghai for Science and Technology, Shanghai 200093, China

[a]liqiangstef@qq.com, [b]zhouzyfj@163.com

Keywords: Road Engineering, Salt Scaling , Glue Spaling , Brine Ice, Concentration of De-icing Salt

Abstract. To study the effect of concentration and type of de-icing salt on salt scaling based on the mechanism of glue spaling proposed by John J. Valenza II and George W. Scherer, the de-icing solution of NaCI and$CaCI_2$ on the concentration of 1%, 3%, 5% and 7% were frozen into brine ice . Order to obtain the relationship of elastic modulus between the type and concentration of de-icing ,all brine ice specimens were tested under uni-axial compressive loading. The test results show: with the increase of concentration, the elastic modulus and peak stress of bring ice were decreased;when the same concentration ,the elastic modulus and peak stress of NaCl brine ice were higher than $CaCI_2$.Based on the test results ,a reasonable explanation of the following phenomenon were given:The different type of de-icing salt all can lead to salt scaling of concrete;when the concentration of de-icing salt is moderate,it is will occur the most serious salt scaling.

Introduction

In the process of concrete salt scaling, the focus of all the researchers is on the effect of the type and concentration of the deicing salt on salt scaling [1-5] : in recent years, new type deicing salt which main composition is $CaCl_2$ began to extensive use, but the effect is not obvious: compared to the concrete road traditional deicing salt is used,the use of new type deicing salt is not improve the durability of concrete ;it is found is not the higher the concentration,the more serious damage of concrete in process of using de-icing salt. Only in low concentrations, the concrete will produce the most severe damage. In this paper, based on the mechanism of glue spaling, unconfined uniaxial loading failure tests was carried on the brine ice which formed by the de-icing solution of NaCI and$CaCI_2$ on the concentration of 1%,3%,5% and 7%.

Salt scaling

Damage phenomenon The research of salt scaling which began in the 1930s is the more early, deeply subject in domestic and foreign. Hundreds of laboratory and field studies have clearly identified the characteristics of salt scaling, but have not explained the cause. In a companion article this work was critically reviewed, and the following list of characteristics was compiled:

Phenomenon (1): Salt scaling consists of the progressive removal of small flakes or chips of binder, and gradually developing inward, exposing aggregate, eventually leading to the scaling damage of the concrete [6].

Phenomenon (2): No matter what the deicing salt, no matter whether the chemical composition, as long as the concentration when appropriate, all can cause serious deicer-frost concrete erosion damage, there is no so-called on concrete harmless deicing salt or snowmelt agent [7].

Phenomenon (3): Regardless of de-icing salt type and chemical composition, as long as the concentration is appropriate, the concrete will cause serious scaling damage. It is not exist the de-icing salt which is harmless to concrete.

Phenomenon (1) show that the strength of the concrete surface affects the extent of salt scaling: the stronger the concrete surface, the weaker the degree of scaling; the weaker the concrete surface, the more serious the damage.Phenomenon (2) and (3) show that salt scaling is related to the physical characteristics and has little to its chemical properties. However, for the phenomenon (3), different scholars have different interpretations [8-9].

Glue spalling mechanism Recently, J.J.Valenza II and G. W. Scherer studied the typical phenomenon of concrete salt scaling and proposed the glue spalling mechanism [6,11]. This mechanism consider the main reason for salt scaling is that the thermal expansion coefficient of ice is about five times to the cement,when the temperature decrease , the deformation of the concrete and ice is not harmonious.The bond strength between ice and concrete is strong enough because the surface of concrete exits micro cracks during use ,thus the interface between ice and cement generates stress. The stress makes the cement mortar of the surface flaking along the existing cracks layer by layer. The cracks expanding and coarse aggregate exposure eventually leads to the concrete scaling.

Text survey

Test content The researchers studied the effect of the type and concentration of the deicing salt on salt scaling mainly from the material properties and mechanical properties of concrete, and ignored the mechanical properties of the brine ice. The glue spalling mechanism considers that the elastic modulus of concrete and brine ice are both related to salt scaling. Gulati and Hagy [12] proposed formulation for the glue spalling mechanism by the finite element analysis:

$$\sigma_{cf} = \left(\frac{E_c}{1-\nu_c}\right)\left[\Delta\alpha\Delta T - \sigma_f\left(\frac{1-\nu_f}{E_f}\right)\right]. \quad (1)$$

$$\sigma_f = \frac{0.5t_c[E_c/(1-\nu_c)]\Delta\alpha\Delta T}{0.5t_c(E_c/E_f)[(1-\nu_f)/(1-\nu_c)]+t_f}. \quad (2)$$

$$\sigma_c = -2\sigma_f\left(\frac{t_f}{t_c}\right). \quad (3)$$

σ is the stress parallel to the x-axis, E is the elastic modulus, ν is the Poisson ratio, $\Delta\alpha = \alpha_f - \alpha_c$ is the thermal expansion mismatch, ΔT is temperature change, and throughout this section the subscripts c and f indicate quantities that correspond to the concrete and ice, respectively. The stresses in the concrete is σ_c, and the ice is σ_f.

Eq.1and Eq.2 only considered the elastic modulus of pure ice. This paper studies the relationship between the type and concentration of brine and the elastic modulus . Unconfined uniaxial loading failure tests was used to obtain the elastic modulus of brine ice . The data from the test was processed and analyzed in order to explain the role of the type and concentration of the deicing salt on salt scaling reasonably.

Test equipment and materials Distilled water and the deicing salt on the concentration of 1%,3%,5% and 7% configured by $CaCl_2$ and NaCI which produced from Sinopharm Chemical Reagent Co., LTD, were used in the test. The refrigerator, STDW-40 low temperature test box is produced from Zhejiang geotechnical equipment manufacture Co., LTD. The loading test apparatus adopts the STH series microcomputer control electro-hydraulic servo universal test machine is from Shanghai sans Measuring Instrument Manufacturing Co., LTD, the whole process can be controlled by microcomputer and data can be automatically storage.

Test method Put the solution of deicing salt into a mould on the size of 4cm×4cm×4cm, and make 9 test blocks formed by the de-icing solution of NaCI and $CaCI_2$ on different concentration. Before the test, the deicing salt solution should be frozen 48 hours in the refrigerator, the freezing temperature is-25℃ , in order to make the temperature of the test blocks can achieve the actual condition of the northeast of our country after the snow.

Take out the test blocks of brine ice from the mould after the frozen, unconfined uniaxial loading failure tests was carried. In the process of loading test, the indoor temperature is controlled at 0℃, in order to reduce the influence of the indoor environment temperature on the results of the test.

According to the research results of the literature [13] , in the process of pressing the brine ice, complete stress-strain curve can be obtained when the rate of the loading test is 10mm/min. So this test loading control method uses displacement control, and loading rate is10 mm/min, the control accuracy of the the same rate is ≤±1%.

Experimental results and analysis

Constitutive relation of deicing salt Contrast Fig.1 and Fig. 2, it is known that the appearance of the brine ice frozen from sodium chloride and calcium chloride solution exists obvious differences: sodium chloride brine ice for thick milky-like, and calcium chloride brine ice for transparent floe in; when it freezes ,the volume expansion of sodium chloride is slightly larger than calcium chloride .

Fig.1 NaCI solution after freezing

Fig .2 $CaCl_2$ solution after freezing

Fig.3 (a) and (b) show the stress-strain curve of NaCl and $CaCl_2$ brine ice in different concentrations when uniaxial compression test without lateral restraint is carried, the results show that:along with the deicing salt solution concentration increases, the peak stress and curve slope of brine ice which is formed by sodium chloride and calcium chloride are both presented down trend; when the concentration is low (1% ~ 3%), the decline degree of sodium chloride and calcium chloride is roughly the same ;with the increase of the concentration, downward trend of the peak stress and elastic modulus of calcium chloride is more obvious and stress-strain curve is more gently which shows that the brine ice of calcium chloride has better ductility.

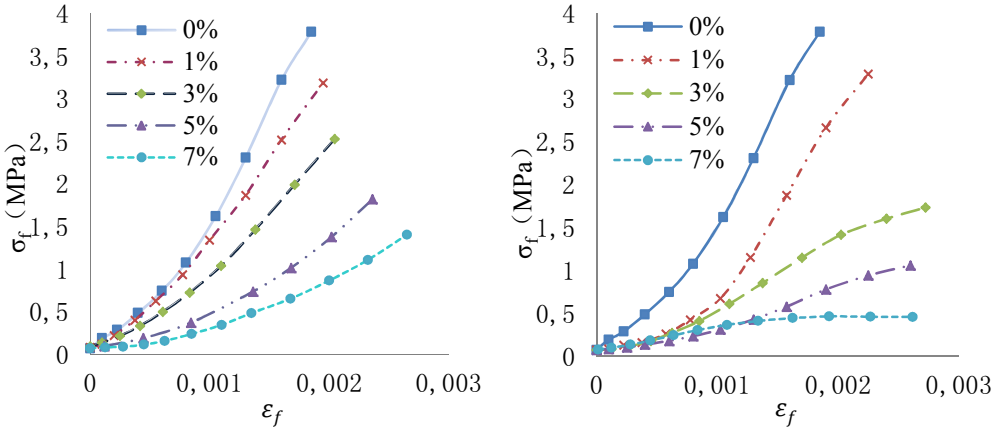

(a) (b)

Fig. 3 Stress-strain curve of brine ice :(a) sodium chloride (b) sodium chloride

The experiment data of sodium chloride and calcium chloride brine ice is processed with the method of regress analysis, it is concluded that a linear relationship between stress and deformation which is showed in Eq. 4 and Eq. 4. The specific parameter values is showed in Table 1.

$$\sigma_f = A\varepsilon_f - B \text{ (Sodium chloride, sample n = 9, correlation coefficient } R_1^2\text{).} \quad (4)$$

$$\sigma_f = C\varepsilon_f - D \text{ (Calcium chloride,sample n = 9, correlation coefficient } R_2^2\text{).} \quad (5)$$

Deicing salt concentration and elastic modulus From the glue spalling mechanism Eq.1 and Eq.2, it is known that in the process of salt scaling, $\sigma_{cs}$and σ_f is directly related to the elastic modulus of brine ice which is E_f: when the concrete elastic modulus, Poisson's ratio, thermal expansion coefficient and the brine ice thermal expansion coefficient ,Poisson's ratio are known, σ_{cs} and σ_f reduce when the elastic modulus E_f decreases. In Fig.2 (a) and (b) the test data is processed with the

method of regress analysis, it is found that the concentration of sodium chloride and calcium chloride and the elastic modulus of brine ice have a good relationship of exponential function, the correlation coefficient are both greater than 0.99, the regression equation is:

$$E_f = 203.36e^{-0.199w} \quad . \tag{6}$$

(Sodium chloride, correlation coefficient $R^2 = 0.9958$)

$$E_f = 204.33e^{-0.353w} \quad . \tag{7}$$

(Calcium chloride, correlation coefficient $R^2 = 0.9957$)

Table 1 The regression equation value of brine ice

para / concentration	A	B	R_1^2	C	D	R_2^2
0%	202.28	0.226	0.9676	202.28	0.226	0.9676
1%	160.83	0.135	0.9834	144.4	0.3452	0.922
3%	118.68	0.102	0.9728	67.841	0.067	0.9839
5%	75.809	0.158	0.9583	39.951	0.0209	0.9715
7%	49.191	0.0847	0.9472	16.321	-0.1208	0.877

Comparing Fig.4 (a) and (b), it is found that the elastic modulus of sodium chloride and calcium chloride are tend to decline with the concentration increases; when the concentration of de-icing salt in 1% to 3%, the elastic modulus of brine ice is relatively close.

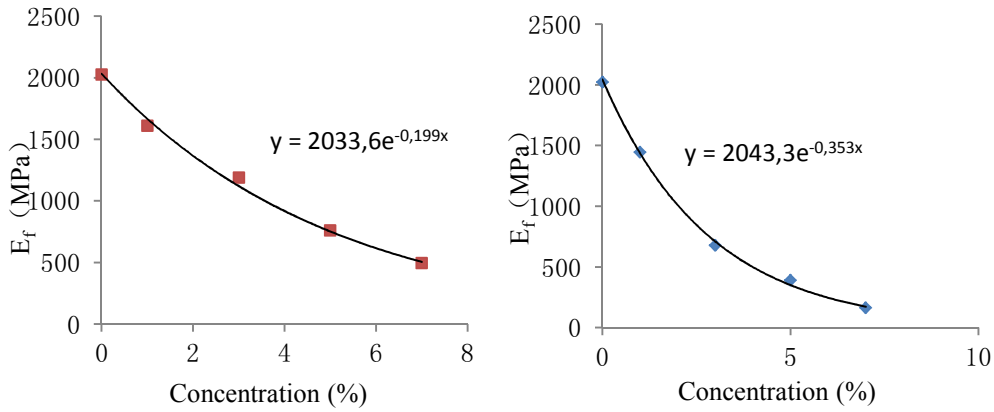

Fig.4 The curve concentration-elastic modulus : (a) Sodium chloride ,(b) Calcium chloride

Freezing sodium chloride or calcium chloride solution,as the temperature decreases , when solution concentration is less than 22.4%, there will be ice precipitation; more than 22.4% ,there will be salt precipitation. Actually, the deicing salt solution concentration is usually far less than 22.4% both in field or laboratory use, so with the temperature decreases there will be ice precipitated from de-icing salt solution and the remaining solution concentration W_L will increase. When the salt solution temperature decrease ΔT, the relationship between the volume of the ice separation in the total volume of the solution Φ and the initial concentration of solution W_0 is[14]:

$$\Phi = 1 - \frac{W_0}{W_L} \quad . \tag{8}$$

Weeks[15] froze NaCl solutions of various concentrations and measured the tensile strength, σ_T. He found the following empirical dependence on the volume fraction of ice, Φ:

$$\sigma_T(\mathrm{MPa}) = 2.47 - 5.15\sqrt{1-\Phi} \quad . \tag{9}$$

Eq.9 indicates that brine ice has no strength below a volume fraction of $\Phi \approx 77\%$ .At the lowest temperature in a salt scaling experiment ($\Delta T \approx 20°C$), ice is in contact with brine at $W_L \approx 22\%$[6]. Using this value in Eq. 8, setting $\Phi = 77\%$, and solving for W_0, indicates that a solution with

$W_0 \geq 6\%$ has no strength in the temperature range of a salt scaling experiment. Through the analysis of Eq.8 and Eq.9, and the relationship between the elastic modulus E_f and concentration in figure 5 and figure 6, we can explain the influence of concentration on salt scaling damage:

With the initial concentration of the salt solution W_0 increases , the tensile strength of brine ice σ_T decrease. When the concentration is low ($\leqslant$ 3%), the tensile strength of brine ice σ_T is larger than the stress σ_f which is produced in the prosess of frozen, so the concrete surface will not occur salt scaling because the brine ice does not damage ;

When the concentration of de-icing salt solution in the medium range (3% to 5%), the stress in brine ice σ_f is larger than the tensile strength σ_T. The brine ice will crack,the scaling stress σ_{cs} in the contact surface between brine ice and concrete which is generated by the temperature changes will be concentration due to the brine ice occur cracks . The stress that increases abruptly is larger than the tensile strength of concrete, which leads to concrete spalling step by step from the surface.

When the concentration of de-icing salt solution is high ($\geqslant$ 7%), the brine ice will occur soften and almost has no tensile strength.The stress that is generated by the temperature changes will be eliminated because the brine ice is too soft ,so the concrete will not occur salt scaling in this condition

Comparison of different solutes Fig. 5 (a)-(d) for comparison of the stress-strain relationship between sodium chloride and calcium chloride r when the concentration is the same . It can be found that when the concentration of the solution is 1% and 3%, the two curves of different solutes are close which indicates that the mechanical properties are close. When the concentration is 7%, in the initial stages of loading, the stress of calcium chloride is larger then sodium chloride ; continue to loading, the stress of sodium chloride is over calcium chloride instead which is showed the sofeten phenomenon of calcium chloride is more obvious. By analyzing Fig. 7- Fig. 10, it can be drawn on the effect of salt type to salt scaling:

The two types of deicing salt solution can both cause scaling damage of pavement concrete. When the concentration of sodium chloride is 3% to 5% ,it will cause salt scaling of the concrete and calcium chloride solution at a relatively low concentration (1% to 3%) can lead to scaling damage to the concrete.

Conclusion

Through the unconfined uniaxial loading failure test on brine ice that formed by frozen deicing solution of different concentration and discussing and analysing on the experimental data, the reason why the concentration of deicing solution is in the medium range during the salt scaling of concrete will cause serious damage is explained: when concentration is low, the stress caused by temperature changes is less than the tensile strength of the brine ice, so the salt scaling can not happen; when concentration is too high, brine ice will happen to soften, have no intensity, the stress caused by temperature changes can not be transfered to the concrete that is lower; when concentration is medium, the tensile strength is large, and can also be transfered to the surface of the concrete, and cause salt scaling on the concrete.

Through the unconfined uniaxial loading failure test on the concentration of de-icing salt with different solute (NaCl and $CaCl_2$), we obtain the effects of the solute: with the increase of concentration of salt solution, the tensile strength and the stress, during salt scaling, of the brine ice that formed by different solute will decrease, as long as the concentration appropriate, it can cause serious stripping on concrete; new solution of deicing salt ($CaCl_2$) did not achieve the ideal effect, after using it, the durability of the concrete will be damaged.

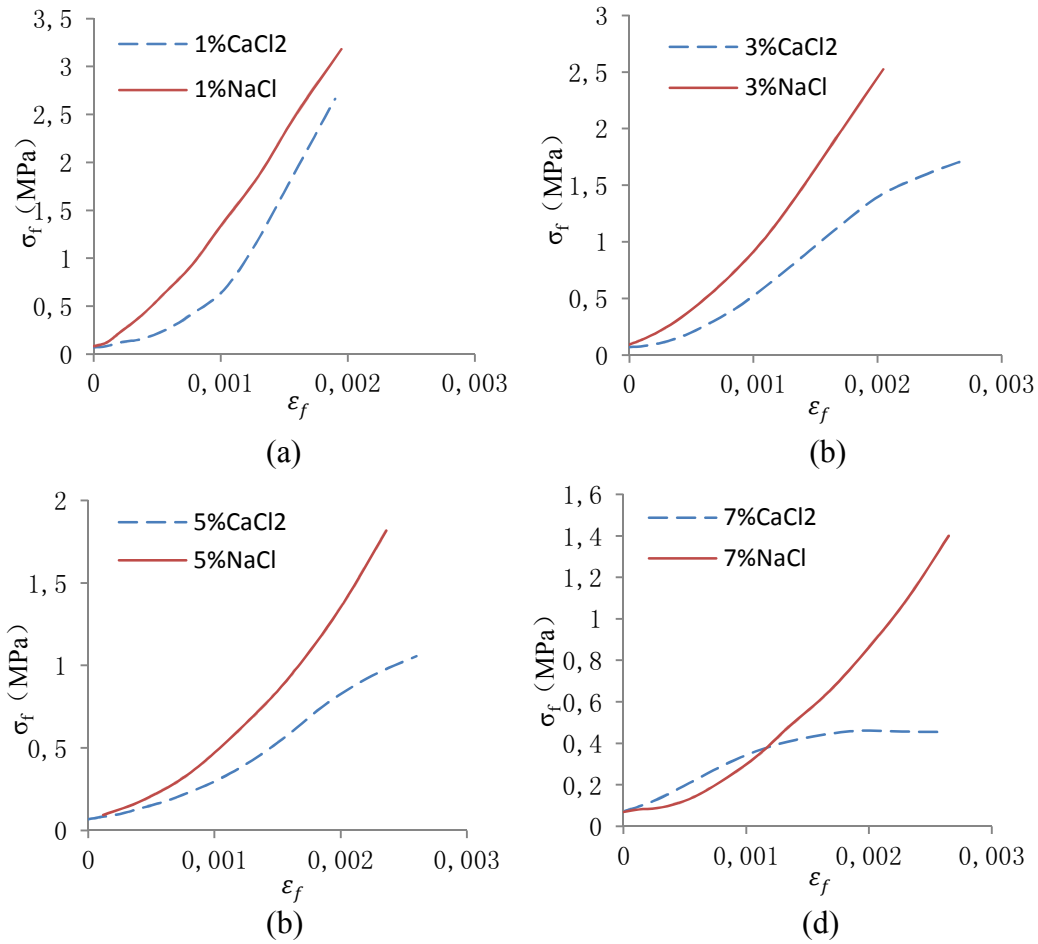

Fig.5 The comparison of different solutes on the concentration of :(a)1% , (b)3% , (c)5% ,(d)7%.

Acknowledgements

This work was financially supported by the Shanghai Natural Science Foundation (09ZR1422200).

References

[1] John J. Valenza II and George W. Scherer.A review of salt scaling: I.Phenomenology. [J]. Cement and Concrete Research ,2007 , 37:1007—1021.

[2] John J. Valenza II and George W. Scherer.A review of salt scaling:II.Mechanisms[J]. Cement and Concrete Research ,2007 , 37:1022—1034 .

[3] Naiqian Feng,Feng Xing.Durability of Concrete and Concrete Structure[M]. Beijing；Mechanical industry press，2009. In Chinese

[4] Zhonghua Li.G. Study on freeze-deicing salt scaling resistance of the pavement concrete in cold region[D]. Harbin Institute of Technology Ph.D. thesis. In Chinese

[5] Quanbin Yang .Concrete salt scaling damage - mechanisms, materials, design and control measures [D]. Tongji University Ph.D. thesis. In Chinese

[6] John J. Valenza II and George W. Scherer. A Mechanism for Salt Scaling[J], The American Ceramic Society:2006,89(4):1161—1179.

[7] Quanbin Yang. Journal of Building Materials :2006,9(4):464-467. In Chinese

[8] J. Marchand, M. Pigeon,D. Bager,and C. Talbot. Influence of Chloride Solution Concentration on Deicer Salt Scaling Deterioration of Concrete[J].Materials Journal，1999,7:429-235

[9] Quanbin Yang. Journal of the Chinese Ceramic Society: 2007,35(1):96-100. In Chinese

[10] Shaofeng Chen,Li Sun and Zhenbao Li. Highway: 2006，4:216—219. In Chinese

[11] John J. Valenza II and George W. Scherer. Mechanism of Salt Scaling[J], Materials and Structures 2005,38 :479-488.

[12] S. T. Gulati and H. E. Hagy. Analysis and Measurement of Glue-Spall stresses in Glass–Epoxy Bonds[J]. The American Ceramic Society,1982,(65): 1–5.

[13] Jinfeng Wang. Low Temperature Architecture Technology : 2007,1:11-13. In Chinese

[14] D. A. Porter and K. E. Easterling .Phase transformations in metals and alloys 2nd edition [M].London; Chapman and Hall,1992.

[15] W. F. Weeks.Tensile Strength of NaCl Ice[J]. Journal of Glaciol, 1962,(4):25–52.

Advanced Materials Research Vols. 450-451 (2012) pp 21-25

doi:10.4028/www.scientific.net/AMR.450-451.21

Theoretical Analysis of Chloride Ion Migration Tests in Cementitious Material Research

Jinbo Yang[1, a], Rengguang Liu[2, 3, b]

[1] Institute of Ecomaterials and technology, College of Materials Science and Engineering, Beijing University of Technology, Beijing 100124, P. R. China

[2] College of Architectural Engineering, Qingdao Agricultural University, Qingdao 266109, P. R. China

[3] Department of Civil Engineering, Key Laboratory of Structural Engineering and Vibration of Chinese Ministry of Education, Tsinghua University, Beijing 100084, P. R. China

[a]jinboyang@bjut.edu.cn, [b] lrg10@mails.tsinghua.edu.cn

Keywords: Ion migration theory, Chloride migration test, Chloride diffusion coefficient, Cementitious material

Abstract. Chloride ion migration tests, or so called electrical accelerated tests, for testing chloride diffusion coefficient of cementitious materials are reviewed. The ion migration theory of electrical accelerated tests is presented. Four main representative measures, chloride penetration test, steady state migration test, unsteady state migration test and salt saturated conductivity test, are introduced and their theoretical calculations of chloride diffusion coefficient are described. Through analysis of the theoretical calculations, it could be found that all electrical accelerated tests are based on ion migration theory although different suppositions are adopted. Steady state migration test is the most suitable measure to determine chloride diffusion coefficient among the migration tests. D_{CIPT}, D_{RCM} and D_{SSCT} calculated by chloride penetration test, unsteady state migration test and salt saturated conductivity test could be used to identify the resistance to chloride ion penetration of cementitious materials but are not the real diffusion coefficient.

Introduction

Chloride ion ingress is a common phenomenon for cementitious materials structure which is in marine environment or in frozen area where deice salt is applied. It will cause reinforcement corrosion for reinforcement cementitious materials structure. The main mechanics of chloride ion ingression include permeation, capillary absorption [1], diffusion, migration and convection. They can be represented by the following mathematic model as Eq. 1 shows. Among them, the convection and migration are always neglected due to velocity of solute is diminutive and migration will only happen in particular case when extra potential is enhanced for example the metro concrete structure. Therefore permeability, sorptivity, and diffusion coefficient are the main three indexes for describing chloride ion ingress hitherto.

$$J = C\frac{k}{\mu}\nabla P + CS\sqrt{t} + D\frac{dc}{dx} + \frac{zUF}{RTl}DC + CV \tag{1}$$

Where J is the chloride ion flux, C is the concentration of the ion source solution, k is the permeability, μ is the viscosity, ∇P is the pressure gradient, S is the sorptivity, t is the absorption time, D is the diffusion coefficient, dc/dx is the concentration gradient, z is the electrical charge of the ions, U is the voltage, F is the Faraday's constant, R is the universal gas constant, l is the distance between electrodes, T is the absolute temperature, V is the velocity of solute.

Diffusion in concrete especially for high performance concrete is a very slow process causes that testing chloride diffusion coefficient is a real time consuming work. In order to determine the diffusion coefficient of concrete rapidly, several accelerated methods were designed in the past 30 years based on the mechanic of migration. In 1981, Whiting [2] developed a method to measure

chloride permeability of concrete. Later, it was accepted as standard method by ASTM C1202 and AASHTO T277 using six hours electrical charge as a rapid chloride diffusion index[3,4], although there is not logical theoretical basis. Essentially it is an unsteady state migration test. There is not a steady chloride ion flux formed across the concrete specimen and it is difficult to indentify how much current is carried by chloride ions. Reference [5] proves that it might be a useful indicator of chloride diffusion and an empirical equation to predicate chloride diffusion coefficient is given by reference [6]. In 1993, an accelerated method called steady state migration test was developed [7,8] and later was accepted as a standard method (NT Build 355)[9]. The steady state migration test using the migration term in Eq. 1 to calculate chloride diffusion coefficient has a clear convincing theoretical basis [8]. However determining chloride ion concentration gradient during the testing procedure is laborious and time consuming and may cause operation error. Until the conductivity sensor was proved experimentally to be a convenient way to determine chloride ion concentration in the anolyte [10] and the theoretical relationship between conductivity and chloride ion concentration was explained by reference [11], steady state migration test is becoming a largely acceptable migration test. As well as an in-situ migration test based on steady state migration test was developed by Basheer [12,13] in 2005. Almost meanwhile, in 1992, Tang and Nilsson [14] devised an unsteady state migration test combining diffusion and migration terms in Eq. 1 to calculate chloride diffusion coefficient by using a numerical solution. Later it was adopted by NT Build 492 [15] as standard method. Although there is a good correlation between steady state migration test and unsteady state migration test [16], the theoretical basis of unsteady state migration test is not acceptable completely due to the migration equation is derived based on steady state migration and whether it is suitable for unsteady state migration is still needed to be proved. In 1995, Streicher and Alexander [17] developed a chloride conduction test for testing the conductivity of high concentration salt solution saturated concrete. And later Lu [18] modified this method by applying Nernst-Einstein equation which is a transformation of migration term in Eq. 1 and which also has been mentioned in reference [7]. For Nernst-Einstein equation, it is difficult of indentify the value of the chloride ion transference number. The perception of making chloride ion transference number equal 1.0 is not reasonable. In 1998, Zhao et al [19] developed an alternating current conductivity test by modifying ASTM C1202 which has been proved correlating well with ASTM C1202 test [19] and unsteady state migration test [20]. This method is devoid of theoretical basis and can only supply an index to evaluate the resistance to chloride ion penetration of cementitious materials. In conclusion, the above chloride ion migration tests are all based on ion migration theory but they give different indexes for describing chloride diffusion coefficient. Therefore which one is approaching the real diffusion coefficient is needed to be identified.

In presented work, the ion migration theory is reviewed and the theoretical calculation of four main tests is analyzed. Through comparison the most suitable test for determining chloride ion diffusion coefficient of cementitious materials is suggested.

Ion Migration Theory

According to electrochemical theory, the electrical driving force on randomly drifting chloride ion in ideal solution is showing in the following equation:

$$f = ze_0 \frac{U}{l} \tag{2}$$

Where f is the electrical driving force (N), z is the electrical charge of the ions (z = 1 for chloride), e_0 is the charge of electron (1.6×10^{-19}C), U is the voltage (V), l is the distance between electrodes (m)。

Then the ion velocity could be calculated as following：

$$v = uf \tag{3}$$

Where u is the absolute mobility (m^2/s/J).

According to Einstein equation[8]:

$$D = ukT \tag{4}$$

Where D is the diffusion coefficient (m^2/s), k is the Boltzman constant (1.381×10^{-23}J/K), and T is the absolute temperature (K).

By combining Eq.2, Eq. 3 and Eq. 4, the chloride ion flux J ($mol/m^2/s$) equals:

$$J = \frac{zUF}{RTl} DC \tag{5}$$

Where F is the Faraday's constant (9.65 × 104 C/mol), R is the universal gas constant (8.31 J/K/mol), C is the concentration of the ion source solution (mol/m^3).

This equation is also named Nernst-Plank equation. If the chloride ion flux could be determined, the chloride ion diffusion coefficient could be calculated with Eq. 5. This is the theoretical basis for chloride migration tests.

Chloride Ion Migration Tests

Chloride Ion Penetration Test

In the chloride ion penetration test (CIPT) following ASTM C1202 specifications, the transport of chloride ions is accelerated by applying an external 60 V direct current voltage. The total charge passing through the specimen during the initial 6 hours is calculated as the resistance to chloride ion penetration which is shown in Eq. 6:

$$Q = \int_0^t I dt \tag{6}$$

Where Q is the total charge (C), I is the current (A), t is the total elapsed testing time (s). If the current is all carried by chloride ion, it will be easy by determining current to calculate chloride ion diffusion coefficient. In fact, in the pore solution of cementitious material there are several ions such as hydroxide ion, calcium ion and sulfate ion will also join the carrying of current. With 6 hours testing time, chloride ion will not pass through specimen in most cases and there will not be a steady chloride ion flux formed. So an empirical equation is applied to predict chloride diffusion coefficient D_{CIPT} (m^2/s) as following [6]:

$$D_{CIPT} = 0.0103\times10^{-8}\times(Q)^{0.84} \tag{7}$$

Steady State Migration Test

In the steady state migration test following NT Build 355 specifications, a 12 V direct current voltage is applied until the chloride ions passing through the specimen. Then the chloride ion flux is determined and chloride diffusion coefficient D_{SSMT} (m^2/s)is calculated by the following equation:

$$D_{SSMT} = J\frac{RTl}{zUFC} \tag{8}$$

Steady state migration is time consuming relatively for continuous measurement of the concentration of chloride ions in the anolyte. Although the conductivity sensor technology can be applied to test chloride ion concentration automatically, several days testing time for getting steady state migration is still needed. However, steady state migration test has a clearly theoretical basis and the chloride ion diffusion coefficient determined approaches the real value closely.

Unsteady State Migration Test

In the unsteady state migration test, also named rapid chloride ion migration test (RCM), following NT Build 492 specifications, a 30 V direct current voltage is applied. Then the chloride ion penetration depth is measured to calculate the chloride diffusion coefficient. In the calculation procedure, both diffusion and migration terms in Eq. 1 are included. The final calculation equation of chloride diffusion coefficient D_{RCM} (m^2/s) is shown below [14]:

$$D_{RCM} = 1.189\times10^{-11}\left(\frac{x_d - 1.062x_d^{0.589}}{t}\right) \tag{9}$$

Where x_d is the chloride ion penetration depth (mm), t is the testing time (hour). It needs to highlight that he RCM test does not need to form a steady chloride ion flux. Therefore the testing time could be shortened to approximately 24 hours.

Salt Saturated Conductivity Test

In the salt saturated conductivity test (SSCT), a solution of 4 mol/l sodium chloride is applied to saturate specimen previously with vacuum dessicator. Therefore a steady chloride flux is assumed to be formed. Then the conductivity is determined by using 5 V direct current voltage. The chloride diffusion coefficient D_{SSCT} (m^2/s), is calculated with the following Eq. 9 [18]:

$$D_{SSCT} = \frac{RT\sigma}{z^2F^2C} \tag{10}$$

Where σ is the conductivity (S/m), C is the concentration of the chloride ion (4×10^3 mol/m^3). With the saturation assumption, a steady chloride ion flux could be seen as formed. The convenience for NEL test is that it can be finished in several minutes except the one day saturation time. Eq. 9 also is a transformation of Eq. 5 by using current to calculate chloride ion flux. During the calculation, the transference number equals 1.0 is assumed although it is obviously not.

Comparison of Different Tests

Hitherto the above-mentioned four tests are the main accelerated measures for determining chloride diffusion coefficient of cementitious materials. In fact, they are not all suitable in theory.

They all based on ion migration theory actually although different assumption is adopted. CIPT test and RCM test belong to unsteady state migration test. SSMT test and SSCT test are steady state migration tests relatively. It is clearly that ion migration theory assumes that a steady ion flux is formed then the voltage distribution could be presumed consistent. In view of this, it is better to apply SSMT test and SSCT test to determine chloride ion diffusion coefficient. Although SSCT test is a steady state migration test, it must be indentified that the current is carried by not only chloride ion flux but also several other ion fluxes such as hydroxide ion flux, hydrogen ion flux and calcium ion flux. Assuming the transference number is 1.0 is not acceptable as reference [13] described. In conclusion, the chloride ion diffusion coefficient tested by the SSMT test is approaching the real diffusion coefficient. On some levels, experiments show that D_{CIPT}, D_{RCM} and D_{SSCT} have a high correlation with D_{SSMT} and they could be used to estimate the resistance to chloride ion penetration of cementitious materials.

Conclusions

The migration tests for testing chloride diffusion coefficient of cementitious are all based on the ion migration theory. The steady state migration test is the most suitable measure to determine chloride diffusion coefficient among the migration tests. D_{SSMT} is the one of all others approaching the real chloride diffusion coefficient. D_{CIPT}, D_{RCM} and D_{SSCT} could be used to identify the resistance to chloride ion penetration of cementitious materials but are not the real diffusion coefficient.

Acknowledgement

This work was financially supported by the UK-China Bridge in sustainable energy and built environment funded to Queen's University Belfast under EPSRC grant No. EP/G042594/1.

References

[1] C. HALL: Mag. Concr. Res. Vol. 41 (147) (1989), p. 51

[2] D. Whiting: Public Roads Vol. 45 (3) (1981), p. 101

[3] American Society for Testing and Materials: ASTM C 1202

[4] American Association of State Highway and Transportation Officials: AASHTO T 277

[5] P.F. McGrath and R.D. Hooton: Cem. Concr. Res. Vol. 29 (8) (1999), p. 1239

[6] P. Ghosh, A. Hammond and P.J. Tikalsky: ACI Mater. J. Vol. 108 (1) (2011), p. 88

[7] C. Andrade: Cem. Concr. Res. Vol. 23 (3) (1993), p. 724

[8] T. Zhang and O.E. Gjorv: Cem. Concr. Res. Vol. 24 (8) (1994), p. 1534-1548.

[9] Nordic Innovation Centre: NT Build 355

[10] M. Castellote, C. Andrade and C. Alonso: Cem. Concr. Res. Vol. 31(10) (2001), p. 1411

[11] P. Yan, J. Yang X. Zhou and S. V. Nanukuttan, in: *STRUCTURAL FAULTS & REPAIR-2010*, edited by M.C. Forde, Edinburgh, Scotland, UK(2010)

[12] P.A.M. Basheer, R.J. Andrews, D.J. Robinson and A.E. Long: NDT and E Int. Vol. 38 (3) (2005), p. 219

[13] J. Yang and P. Yan: J. Adv. Concr. Technol Vol. 7 (3) (2009), p. 385

[14] L. Tang and L. Nilsson: ACI Mater. J. Vol. 89 (1) (1992), p. 49

[15] Nordic Innovation Centre: NT Build 492

[16] L. Tong and O.E. Gjørv: Cem. Concr. Res. Vol. 31 (7) (2001), p. 973

[17] P.E. Streicher and M.G. Alexander: Cem. Concr. Res. Vol. 25 (6) (1995), p. 1284

[18] X. Lu: Cem. Concr. Res. Vol. **27** (2) (1997), p. 293

[19] T. Zhao, Z. Zhou, J. Zhu and N. Feng: Cem. Concr. Res. Vol. 28 (1) (1998), p. 7

[20] J. Yang, F.H. Wittmann, T. Zhao: Restor. Build. Monum. Vol. 16 (1) (2010), p. 57

Advanced Materials Research Vols. 450-451 (2012) pp 26-29

doi:10.4028/www.scientific.net/AMR.450-451.26

Synthesis of Poly L-glutamate Initiated by Triethanolamine

Zhiming Zhang [1,a],Shiqian Wei [2,b], TingTing Li [1,c] and Lihua Han [2,d]

1 Hebei Province Key Laboratory of Inorganic Nonmetallic Materials, College of Materials Science and Engineering, Hebei United University, Tangshan, 063009, China

2 College of Chemical Engineering, Hebei United University, Tangshan, 063009, China

[a] benjamming@heuu.edu.cn, [b]shiqian354298@163.com,

[c] stopstopli2005@sina.com, [d] tshlh@heut.edu.cn

Key words: Triethanolamine; Ring-opening polymerization; Poly-l-glutamic acid

Abstract With L-glutamic acid as raw materials, N-carboxy-L-glutamic acid-benzyl-anhydride (BLG-NCA) was synthesized by triethanolamine. With triethanolamine as the initiator in the anhydrous dichloromethane, ring-opening polymerization of BLG-NCA was initiated, poly-l-glutamic acid benzyl ester was obtained. The amount of initiators, molar ratio of monomer/initiators, reaction temperature and reaction time to the effect of poly-l-glutamic acid benzyl ester in the ring-opening polymerization of BLG-NCA were studied. At last, poly L-glutamate was got, after the debenzylation in HBr solution. Through infrared spectroscopy, Ubbelohde viscometer, ^{1}H NMR spectra, polymerization product was characterized and analysized. Results showed that in dichloromethane, ring-opening polymerization of BLG-NCA could be initiated by triethanolamine.

Introduction

Polyamino acid (such as polyglutamic acid, polyaspartic acid, polylysine, etc) has a structure of amide bond which is similar with protein, it is a kind of biodegradable material. Polyamino acid has excellent biocompatibility, because in carboxylic molecules one or more than one hydrogen atom are replaced by amino group. Poly L-glutamic acid (PLGA) is a kind of polypeptide copolymers, and it is connected by amides bond which is located between alpha amino and carboxyl group in L-glutamate. It has good compatibility with cells, tissues and other biological components, it is easily degraded, metabolism and absorbed into the body and no side effects in living bodies. Because there are a lot of carboxyl in its molecular chain, it is easy grafting or blending with other polymers, and forming a more excellent properties of materials, thus it has been widely used for drug slow-release[1-3], medical adhesive and other tissue engineering[4], etc.

In this paper, with L-glutamic acid as raw material, BLG-NCA is synthesized by triphosgene. With triethanolamine as the initiator, ring-opening polymerization of BLG-NCA is initiated by triethanolamine. Poly-l-glutamic acid benzyl ester is got, studying on the amount of initiators, molar ratio of monomer/initiators, reaction temperature and reaction time to the effect of poly-l-glutamic acid benzyl ester in the ring-opening polymerization of BLG-NCA. Poly L-glutamate is got,after the debenzylation in HBr solution and the structure is characterized.

Experimental process

In a dry flask with three, a new synthesis of BLG-NCA[5]was introduced, according to the rate of charge(triethanolamine is not dissolved in dichloromethane at normal temperature,so it needs diluted by propanone before experiment), the measurement of aniline and 30mL dichloromethane

are added, they are reflowing under nitrogen and mixed reactions. Reaction solution was poured into excessive amounts of alcohol, then it was precipitated and filtered. After natural drying, transparent solid polymers are got. Its yield is common.

After 1.0g new synthesis of PBLG was prepared, it is dissolved by 16mL trifluoroacetic acid at 50˚C, and then 7mL volume fraction of 33% HBr-acetic acid solution are added, they were maintained at 50˚C, 2h, at room temperature overnight. Reaction solution was slowly poured into 300mL ether, it is precipitated and filtered. After drying, 0.52g PLGA was got. FT-IR spectrum was measured with a Nicolet-380 Fourier Transform Infrared Spectrometer. 1H NMR spectra is measured with a Bruker Unity-400 NMR spectrometer, the solvent is CDCl3, and internal standard is the four methyl silicone. The intrinsic viscosity of samples [η] is determinated by Ubbelohde viscometer with a point method.

Result and discussion

Ring-opening polymerization of NCA was initiated by triethanolamine in dichloromethane. Ring-opening polymerization process is shown in Fig.1. 5-carbonyl carbon atom of the NCA monomer was attacked by the tertiary amine of triethanolamine, just as triethylamine, intermediate was formed. Then the intermediate rapidly eliminated CO2 and continued to react with another NCA. The assynthesized polymer was then dried vacuum at 50˚C for 24h.

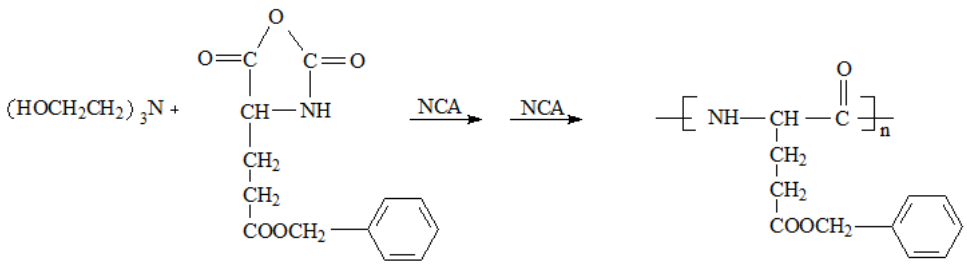

Fig.1 Reaction path of poly-L-glutamic acid benzyl ester.

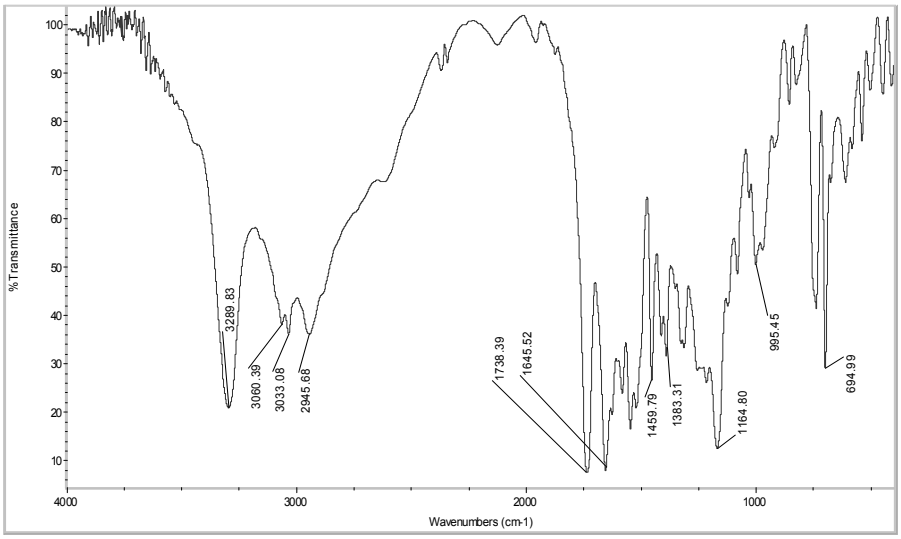

Fig.2 FT-IR spectrum of poly-L-glutamic acid benzyl ester.

FT-IR analysis of Poly L-glutamate assynthesized is represented in Fig. 2. Peaks at 3290, 1646 and 1549 cm-1 are associated with the secondary amide characteristic absorption peak in the polymer. The peak at 3290 cm-1 is designated as the stretching vibrations of N-H of the amide. The peak at 1646 cm-1 is designated as the stretching vibrations of C=O of the amide, the amide I. The

peak at 1549 cm-1 is designated as the asymmetric stretching and symmetric vibrations of CH2 stretching vibrations of C=O of the amide, the amide II. The characteristic absorption peak at 1865cm-1, 1774cm-1, 930cm-1 was disappeared, which indicated that BLG-NCA was polymerized.

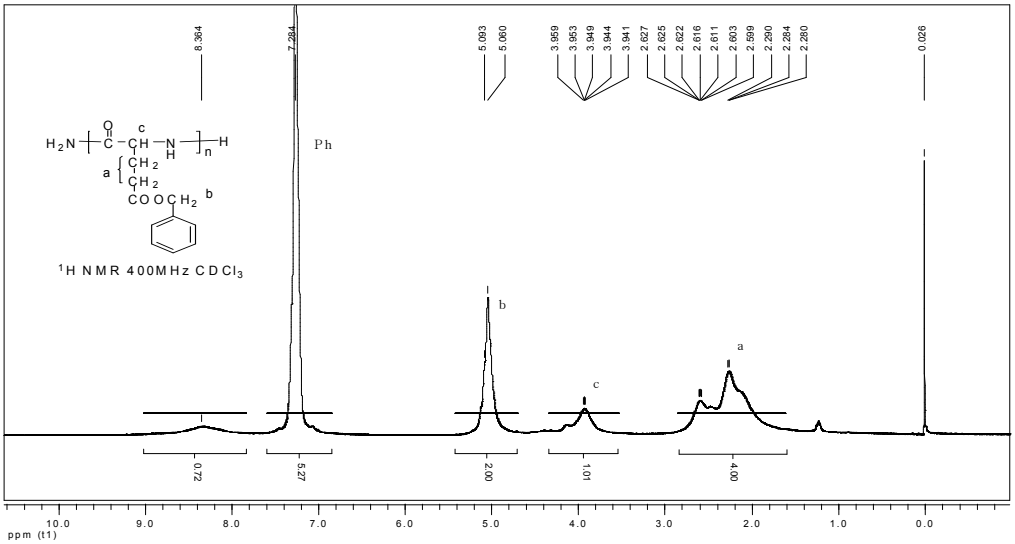

Fig.3 ^{1}H NMR spectra of poly-L-glutamic acid benzyl ester.

In Fig.3 about 1H NMR spectra, at about δ 2.28 chemical shift of β-proton of methylene comes forth. And at about δ 2.62 chemical shift of γ-proton of methylene appears. The peak of about δ 3.95 agreed to the chemical shift of α-proton of methine. At about δ 5.06 chemical shift of the proton of the methylene in benzyl group.While the chemical shift of benzene ring at about δ 7.2 is masked by that of CDCl3. Fig.3 shows PBLG was synthesized.

Table 1. The intrinsic viscosity & viscosity average molecular weight of PBLG

No.	t_1	t_2	t_3	t_4	η_r	η_{sp}	[η]	[M]
1	31.04	31.15	31.21	31.13	1.118	0.118	2.48	11958

The solvent of PBLG of sample on viscosity measurement is N, N-dimethylformamide (DMF), the experimental temperature is 25 ˚C and the molecular weight is calculated with [η]=2.9×10-7M1.7 [7]. It can be seen that in Table 1 the molecular weight is proportional to the intrinsic viscosity [η]. The solvent of PLGA of sample was the 0.4mol/L NaCl and 0.01mol/L NaH2PO4 solution, the experimental temperature was 25 ˚C,and the molecular weight was calculated with [η]=2.95×10-5M0.94 [3]. Viscosity-average molecular weight of the polymer is about 12000 measured which is more than that initiated by triethylamine.

Summary

In summary, BLG-NCA was firstly polymerized initiated by triethanolamine in this work through infrared spectroscopy, Ubbelohde viscometer, 1H NMR spectra. Three hydroxyl of triethanolamine might hinded the nucleophilic attack of ring-opening polymerization. All these results indicate that compounds with functional groups have great potential in the study of the mechanism of this polymerization initiating with lots of nucleophile.

Reference

[1] Bryant SJ, Nuttelman CR, Anseth KS. Cytocompatibility of UV and visible light photoinitiating systems on cultured NIH/3T3 fibroblasts in vitro[J]. Journal of Biomaterials Science, Polymer Edition, 2000, 11(5): 439.

[2] Jeong YI, Sun HS, Shim YH et al. Nifedipine encapsulated core-shell type nanoparticles based on poly (γ-benzyl L-glutamate)/poly (ethylene glycol) diblock copolymers[J]. Journal of microencapsulation, 2004, 21(4): 445.

[3] Sugimoto H, Nakanishi E, Hanai T et al. Aggregate formation and release behaviour of hydrophobic drugs with graft copolypeptide-containing tryptophan[J]. Polymer international, 2004, 53(7): 972.

[4] Deming TJ. Synthetic polypeptides for biomedical applications[J]. Progress in Polymer Science, 2007, 32(8-9): 858.

[5] Li Liying. The Assembly Synthesis of Materials-based on Polymer and Anionic Surfactant [D]. Institute of Chemical, Nankai University, Tianjin, (2008),p.44

[6] Cao Tian, Yin Jingbo, Luo Kun, Chen Hongdan, Chen Xuesi. Synthesis and Characterization of Poly-L-glutamic Acid with a High Molecular Weight [J]. Chemical Journal of Chinese Universities,Vol.27(2) (2006),p.369

[7] He Manjun, Chen Weixiao, Dong Xinxia et al. Polymer physics [M], Fudan University Press, Shanghai, (1983), p.105

Advanced Materials Research Vols. 450-451 (2012) pp 30-33

doi:10.4028/www.scientific.net/AMR.450-451.30

Experimental research on the separation and recycle of waste concrete

Ri Hua Zhang

Luoyang Institute of Science and Technology, Luoyang, Henan 471023, China

zhangrihualy@126.com

Keywords: Waste concrete, Separation, Shelling, Recycled coarse aggregate, Fines.

Abstract. Concrete is the largest amount of artificial building materials in the world today. According to incomplete statistics, the construction waste produced in china each year can reach about one hundred million tons, and it can reach hundreds of millions of tons due to the long accumulation, which has become a serious social and environmental issues. In this paper, the technology of separation and recycle of waste concrete is studied, and the components of waste concrete are separated effectively, which provides a technical guarantee for the recycling of waste concrete.

The waste concrete is disposed through the process of crushing, shelling and sieving and so on, the coarse aggregate and fine aggregate are separated effectively, the properties of coarse aggregate are nearly the same as natural aggregate. When the shelled fines is milled into ultrafine powder and used as concrete admixture, the performance of concrete can be improved. These all provide a new effective way for the recycling of waste concrete.

Introduction

Concrete is the largest amount of artificial building materials in the world today, and about 1.5~2 billion m^3 of concrete are poured in China each year. At the same time, urban renewal construction will demolish some aged buildings, which result in the amount of waste concrete more and more. On a conservative estimate, nearly 100 million tons of waste concrete are produced in China and more than one billion tons of waste concrete are produced all over the world.

The discard of waste concrete itself is a waste of resource, it has become a serious social and environmental issues. At present, the method of disposing the waste concrete is single, the way of simple landfill is generally adopted, some research work on the recycling of waste concrete is also performed. But overall, the disposal of cement-based solid waste is still in no use or low-lever use stage. It not only results in an enormous waste of resources and energy, but also brings damage to the environment even has adverse effects on the development of national economy and the construction of harmonious society. Therefore, the recycling of construction waste becomes more and more important and urgent.

In this study, the coarse aggregate and fine aggregate as well as hardened cement paste in the waste concrete are separated effectively, coarse aggregate is reused for producing new concrete, and other fines are used as concrete admixtures after grinded.

"Shelling" separation process of waste concrete

For the waste concrete from demolition site, coarse aggregate and fine aggregate are tightly cemented together by hardened cement paste and have certain strength. Adopting the ordinary method of crushing can only crush the waste concrete on the size, coarse aggregate and fine aggregate can't be separated effectively. In order to achieve good separation effect, coarse aggregate and fine aggregate must be separated, that is similar to husk the "shell" on the surface of coarse aggregate, thus obtain the coarse aggregate with clean surface, sand and cement mortar as well as other mixtures.

A specialized device of separating concrete called waste concrete sheller is developed in this study. It can complete the "shelling" separation of waste concrete which particle size is not more than 40mm. The principle is that applying mechanical method to effectively grind the certain size of waste concrete, thus strip the hardened cement mortar from the surface of coarse aggregate. Specific separation process is shown in Fig.1.

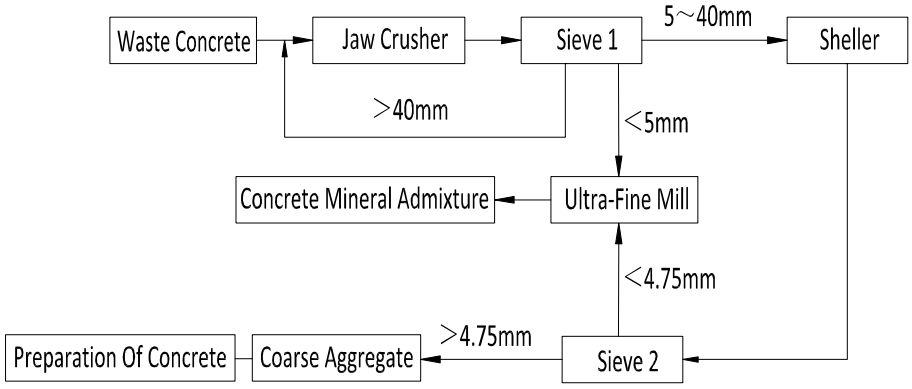

Fig.1 Flow chart of the separation process of waste concrete

"Shelling" separation effects of waste concrete

Coarse aggregate and "shell" are obtained by the "shelling" disposal of waste concrete. The main components of "shell" are cement mortar and small particle size of stones and so on. The separation effect is mainly determined by the amount of coarse aggregate and its properties. In the process of "shelling", if all the coarse aggregate can be restored, the effect is the best. But it is impossible, because in the process of crushing, "shelling" and separating, some coarse aggregate become smaller (less than 4.75mm), meanwhile, the "shelling" time also has effects on the amount of coarse aggregate.

The shelled mixtures are sieved by the round hole sieve, the diameter of the round hole is 4.75mm. The aggregate which particle size greater than 4.75mm is called "shelling" coarse aggregate, it will be used as coarse aggregate for producing new concrete. The mixtures which particle sizes are less than 4.75mm are the "shell" of waste concrete, it is called fines. When the fines are grinded by the ball mill to the specific surface area more than 400m^2/kg, it can be used as concrete admixture.

The test results of "shelling" and sieving are shown in Table 1, the mix proportion of waste concrete in test is shown in Table 2, the strength grades of concrete is C30, service time is about 10 years.

Table 1 "Shelling" separation effect of waste concrete

Shelling time[min]	Coarse aggregate [%]	Fines [%]	Coarse aggregate: fines
2.5	61.6	38.4	1.62:1.0
4.0	54.0	46.0	1.17:1.0
5.0	41.2	58.8	1.0:1.40
7.5	26.0	74.0	1.0:2.84
10	21.0	79.0	1.0:3.76
Actual value	52.6	47.4	1.11:1.0

Table 2 Mix proportion of raw material of waste concrete[kg/m^3]

Ingredients name	Stone	Sand	Cement	Water
Used material	Gravel	Medium sand	P.C 32.5	Tap water
Mix proportion	1273	520	448	179

Property testing of being shelled coarse aggregate

Perform associated property testing on the "shelling" coarse aggregate and shelled fines, and compare with natural aggregate and recycle aggregate without "shelling", the results are shown in Table 3 and Table 4.

Table 3 Property of recycled and "shelling" recycled coarse aggregate and natural graval

Lndex	Material		
	Recycled coarse aggregate	"Shelling" coarse aggregate	Natural gravel
Bulk density[kg/m^3]	1180	1495	1580
Apparent density[kg/m^3]	2370	2391	2440
Voidage [%]	50	41	35
Crush index[%]	11.3	6.4	4.4
Water absorption[%] [24h]	6.4	1.4	2.6

Table 4 Comparison of particle size distribution[%]

Type of coarse aggregate	Particle size range[mm]		
	5-10	10-20	20-30
Recycled coarse aggregate	12.56	50.76	36.68
"Shelling" coarse aggregate	15.68	59.26	25.06
Natural gravel	14.36	46.68	38.96

Properties of concrete produced in coarse aggregate and fines separated from waste concrete

In order to test the influence of "shelling" coarse aggregate and grinded fines to the properties of concrete, related experiments are performed and the specific results are shown in Table 5. Where, benchmark concrete is produced by natural aggregate, the specific area of "shelling" fines is 430m^2/kg, the grades of ground slag is S95.

Table 5 Comparative tests of concrete of different mixtures

Number	Category	Admixture [%]	Slumps [mm]	Compression strength [Mpa]	
				7d	28d
1	Benchmark concrete	0	70	31.7	40.9
2	"Shelling" coarse aggregate as admixture	0	75	35.0	51.5
3	Shelled "shelling" fines as admixture	15	100	34.8	45.5
4	Ground slag as admixture	15	100	28.5	50.5
5	Shelled "shelling" fines and ground slag as admixture[1:2]	15	90	32.9	52.9

Results Analysis

(1) The influence of "shelling" time to separation effects. Table 1 shows that the amount of produced "shell" increases with the growth of "shelling" time, which indicates that the cement paste and the easy crushed aggregate on the surface of recycled coarse aggregate fall off, and the appearance shape of coarse aggregate is very smooth and has been similar to natural gravel. The test results also show that there is an optimal "shelling" time range, 4.0~5.0 min, then the ratio of coarse aggregate to fines is close to the actual mix proportion of concrete.

(2) The test results in Table 3 show that the property indexes of "shelling" coarse aggregate such as density, voidage, crush index and water absorption are better than those of the recycle coarse aggregate which is crushed and sieved only one time. The property indexes of "shelling" coarse aggregate is close to that of natural aggregate, especially the crush index, it is nearly the same as natural aggregate after "shelling". Table 4 shows that the particle size of aggregate becomes smaller after "shelling", which is related to grinding effect.

(3) The test results in Table 5 show that the property index of concrete produced by "shelling" coarse aggregate is improved, it is mainly because the appearance shape and size grading of "shelling" coarse aggregate are improved. After the "shelling" fines are grinded, one kind of product called "shelling" fine powder which is similar to ground slag is obtained. If the "shelling" fine powder is used as concrete mixture, the properties of concrete will be improved significantly. If the content of admixtures are the same, compared with the concrete which use ground slag as admixture, its early strength is high and later strength is low. This is determined by the composition of "shelling" fine powder. Compared with ground slag, its active ingredient is less and the composition of sand is more, which result in its low contribution to the later strength of concrete. If the sand is separated, its activity will increase.

Conclusion

Applying mechanical method to effectively grind the waste concrete, the hardened mortar can be shelled effectively from the surface of coarse aggregate, the ideal coarse aggregate can be obtained, which can improve the properties of concrete. The fines is a good kind of concrete admixture after grinded.

Acknowledgements

The supports from Application Technology Research and Development Projects of Luoyang city under Grant NO. 1101039A is gratefully acknowledged.

References

[1] S.G.Hu and Y.J.He:Journal of the Chinese Ceramic Society. Vol. 35 (2007) NO.5, p. 593. (In Chinese)

[2] H.W.Wan, X.F.Zhong and Z.H.Shui: Science and Technology of Overseas Building Materials. Vol. 26 (2005) NO.2, p. 1. (In Chinese)

[3] R.H.Zhang, J.S.Liu and D.H.Qian: Patent ZL200820069815.5 (2008) (In Chinese)

Advanced Materials Research Vols. 450-451 (2012) pp 34-37

doi:10.4028/www.scientific.net/AMR.450-451.34

Research and development progress on concrete preparation with seawater

Liu Ruicui[a], Jiang Fuyi[b], Liu Ziquan [c,*]

School of Environmental and Material Engineering, Yantai Universiy, Yantai, Shandong, 264005, China

[a]liurc1@163.com, [b]fyjiang@163.com, [c,*] lzqytu@163.com

Keywords: Seawater, Mixing Water, Concrete, Cement.

Abstract. This document outlined the development of concrete mixing water at first. And then it discussed some properties of concrete prepared with adding sea water and impacts of sea water on effectiveness of concrete. The article also tried to explain some reasons of these impacts. The author emphasized on analyzing the effect to the function of concrete by using seawater as mixing water and the reasons and separately elaborated on the different effects to plain concretes and reinforced concretes. At last, the article predicted the development trend of using seawater as concrete mixing water.

Introduction

In general, drinking water is used as the mixing water of concrete, such as running water, the flowing river water or lake water etc. Those that affect the common usage of concrete and invariability are not suitable for using such as sewage, marsh water and so on. While China relatively lacks in freshwater, water per head is only 2400 m^3, only about 1/4 of the world average, ranking 109 in the world. China has been listed one of the 13 countries who have less water per head by UN. Of the 660 cities in China, more than 300 cities lack water. But China is rich in seawater resources and its coastline is as long as 18 thousand kilometers [1]. If they are exploited, they will make up for the shortage of freshwater to a certain extent. So in daily industrial production and life, they need to actively find a breakthrough point to replace freshwater with seawater, striving to play a role in the sustainable development. Up to now, the annual production of cement in China has been over 1 billion tons which is over half of the total production in the world. Every year mixing such a great number of cement needs to consume billions tons of water. If the water is all running water or other forms of freshwater, it would be a heavy burden for a country relatively short in freshwater. Furthermore, for some regions such as sea-island, salt lake, seaside or others, freshwater is more scarcely. It is more urgent to use non-freshwater to mix concrete in these regions. So some researchers studied on the mixing water sorts in concrete production industry.

Evolution of water in concrete product

Usage of recycled water. Recycled water refers to the non-drinking water that reaches the mandated standard after disposal and can be used in life, municipality, environmental and so on. Reclaimed water has different standards and uses according to the different water qualities. The mixing water of concrete is a major part of construction water, and it is a great amount compared with various industries. Now most of the mixing water is running water, namely drinking water. While China is among the 13 countries which lack in water, under the current circumstances, using a lot of drinking water for mixing water is a great waste of water, and so that need to seek a way to recycle water resources. China national standard 《Building design specifications of recycled water》(GB50336 - 2002) and 《Recycling of urban waste water and quality of urban miscellaneous water 》(GB/T18920 —2002) firstly include reclaimed water in building operations, or the mixing water of concrete contain recycled water, while it requires that mixing water conform to the according regulations in another China national standard 《Concrete Water Consumption Standard》 (J GJ63 —89) too[2].

Use of water reducing agent. Water reducing agents of concrete are practically the most important part of the additives. Under the circumstance of constant fluidity, adding water reducing agents can enable to use less water in concrete production, so as to improve the intensity and durability of concrete. The application of water reducing agents is a great leap as it not only reduces the amount of water used but also to improve the performance of concrete [3].

Current situation of using sea water to produce concrete. Some technology departments in the world side had developed blending agents that could make seawater mix concrete. A kind of chemical blending agent developed by a London Concrete High Technology Company could improve the performance of cement so as to enable seawater and unwashed underwater sandstones to mix reinforced concrete. This new product had been used in the Reinforced Concrete Wall Project of French South Pacific islands nuclear test site, Monaco, basic pier projects of port structures and coastal constructions of some other countries, and it has got a good feedback. Now a series of blending agents that can be used for using seawater to mix concrete appear, and the price go down, they also make Technical Supervision Departments of a few countries allow the coastal constructions to use seawater to mix concrete, for example, a contractor in America has listed using seawater to mix concrete in the Category of Technology. Coastal people of the Middle East are more interested in this technology. In the future, on the base of producing cheap and high-quality blending agent, using seawater to mix concrete will be promoted more widely [4,5].

Research on magnetic water. At the moment many scholars and researchers from China and abroad are testing and applying the technology of magnetic water to produce concrete, this technology can increase the intensity of concrete by 10~25 percent, so it can save cement. According to the test by our country, using magnetic water to mix cement and concrete, the usage of cement decreases by 10 percent, while the intensity of cement doesn't decrease, instead it increases by 10 percent. Many construction departments in former Soviet Union have applied the usage of magnetic water to produce concrete and they have achieved great economic benefits, for instance, on the Saratov construction site, using magnetic water to produce concrete enables the intensity of concrete to increase by 14 to 17 percent, while the usage of cement decreases by 12 percent [6].

The impact of seawater on paste matrix and the performance of concrete

Seawater is not pure, although as different areas are different in the kinds of salt in the seawater as a result of different geological, climate and hydrologic conditions, the ratio of different kinds of salt are similar, i.e. NaCl accounts for the most, chloride accounts for 85 to 89 percent, sulphate ranks the second [7]. In addition, seawater includes nitrate, phosphate, carbon dioxide, bromide salt, iodized salt, malysite and son on. They exist in seawater as ions. The pH of seawater fluctuates between 7.7 and 8.5. Concrete is a heteropic, polynary, spongy, vapor-liquid-solid compound material that is produced by the mixing and hardening of cementitious materials, coarse aggregates and sand. Under the effect of water pressure and capillarity, the water can permeate the concrete, like seawater and cement have hydration and produce paste matrix. After a series of complex physical and chemical reactions, concrete structures are eroded. Carbonization of concrete is another kind of chemical erosion to concrete [1, 8, 9].

The components in seawater that affect the performance of concrete are mainly chloride ion, sulfate, Mg^{2+}, carbon dioxide and so on. In the concrete Cl^- could react with calcium luminate in unhydrated cement to produce $3CaO{\cdot}Al_2O_3{\cdot}Ca_2Cl_2{\cdot}10H_2O$. Also chloridion could permeate the concrete by pores, if the concrete is not close-grained, it will result in the erosion of steel bar in the reinforced concrete, so the concrete breaks. While for the plain concrete, as Cl^- exists, it may slow and weaken the erosion of concrete by seawater. So we did not need to consider the negative impacts on plain concrete by chloridion in the seawater. The erosion of SO_4^{2-} is by hydration. Generally speaking, this kind of product will expand and make concrete crack and expand, but that kind of phenomenon doesn't happen in sea concrete. In seawater Mg^{2+} reacts with $Ca(OH)_2$ in paste matrix, producing $Mg(OH)_2$ which has a bad solubility. These $Mg(OH)_2$ stay on the surface or cracks of the concretes, they may slow the erosion of sulphate. The feature of the erosion caused by Mg^{2+} is that the process mainly happens on the surface of the concrete, Mg^{2+} accumulate on the

surface in the form of $Mg(OH)_2$. The impact is so little that it can be ignored in the process of conserving concrete. There is little carbon dioxide in normal seawater, while under special conditions, seawater can have a large amount of carbon dioxide, and it will become more erosive. That is because carbonic acid is more acidic in seawater compared with in water with low salt content. While in normal seawater, hardened cement undertake carbonization and only produce covering layer on the surface of concrete. So we could think that this erosion is slight and can be omitted [1, 7].

In a narrow sense, concrete is a compound material which is made by mixing water, sand, coarse aggregates and cement with a certain ratio. If the concrete has steel bars, it is called reinforced concrete. However, plain concrete refers to concrete without steel bars. Cement mortar is made by mixing water, cement and sand, without coarse aggregates. Aggregates include sand and stone, sand is the fine aggregate while stone is a kind of coarse aggregate. Cement mortar could only be used as the binding material in the masonry construction, it doesn't need stones but a certain number of sands are needed.

The difference between using seawater and using water with low salt content to produce concrete is that there are some kinds of salts in the seawater, and they have a few influences on the performance of concrete. But through the test and numerous surveys some researchers had fond that seawater mixing had a little effect on the intensity of plain concrete, it was similar to adding inorganic salts to the concrete and improves the early intensity of it. As normally seawater has a relatively small amount of inorganic salt ions, seawater mixing has a little effect on the latter part [1]. The clause 3.6.2 of 《The Job Specification of Concrete in Marine Traffic Engineering》 issued by the Ministry of Communications in China regulates that seawater could be used to preparing plain concrete in areas that lack water with low salt content, for those that have a demand for frost resistance, the cement water ratio should decrease by 0.05. A large number of tests and practices of using seawater and water with low salt content to producing plain concrete showed that using seawater performs almost as well as water with low salt content.

Using seawater to manufacturing reinforced concrete: The compulsory entry 3.1.7 of 《The Standard of Water for Concrete》 [10]regulates that untreated seawater are forbidden in reinforced concrete and prestressed concrete. Untreated seawater cannot meet the technological demand for water to produce concrete. The salt content in the sea could be over 3000mg/l, especially the chloridion, it could be over 15000 mg/l. High salt content will affect the performance of concrete and it will specially affect the intensity of concrete severely. For example, high Cl^- content will cause the erosion of steel bars in concrete, destroying the structure. So it is forbidden for untreated seawater to be used to mix reinforced concrete and prestressed concrete. While with the development of concrete preparing technology, using seawater to produce concrete had become a reality. For example, the Concrete High Technology Corporation in London in England developed a chemical blending agent called Z-12öC, it may improve the performance of cement, so it could enable seawater and unwashed sandstones at the bottom of the sea to prepare concrete. It is reported that the blending agent is made by the mixing of 18 inorganic chemicals. It was put to mass produce in the Concrete High Technology Corporation in London in England in 1988. This new product has been used in the Reinforced Concrete Wall Project of French South Pacific islands nuclear test site, Monaco, basic pier projects of port structures and coastal constructions of some other countries, and it had got a good feedback. The results showed that the concrete mixed by that blending agent and seawater had good workability and it also had a smaller poriness and fewer cracks. It had a shorter freezing period, was dry on the surface and as sleek as porcelain. And the agent can form an inorganic compound protection layer on the surface of the steel bar to stop the trend of erosion by chloridion [4, 5].

The research group of M. Zhang etc [11] tested the mechanical property of the concrete mixed with seawater and other kind of water with a low salt content on the basis of comparing the colloidal mortar strength between them. Analysis of the experiment result of cement showed that there were few differences volume of using water in standard consistence and stability of volume between using fresh water and sea water. But the former test sample freezes much earlier than the

later. The other concrete's tests showed that the two kinds of concrete differ little in intensity, but concrete mixed and conserved by seawater are relatively less intensive and there were pronounced frosts. So that concrete mixed by seawater should be conserved by water with low salt content in construction. The mixing proportion of using seawater to produce concrete could be the same as using water with low salt content.

Conclusions

Although at present researches from domestic and abroad had been conducted on using seawater to prepare concrete, but these researches mainly focus on what kind of additives in the seawater could improve the performance of concrete. We think that there have to be researches in the following aspects, for example, how to improve the basic components of paste matrix, how to improve the compactness of concrete, study on the permeability admixture of concrete, research on inhibitor of the steel bar, exploring on decreasing the charges passed of concrete and developing on the treatment of the surface of concrete.

Acknowledgement

This work was supported by "Science and technology project of Shandong provincial department of education.（J08LA11）" and "Promotive research fund for excellent young and middle-aged scientists of Shandong Province（2008BS05006）".

References

[1] B. Guo, B. Wang: Low Temp. Arch. Technology Vol.1 (2005), p.11

[2] W. Ding, F. Leng, D. Ma: Concrete Vol.6 (2005), p.23

[3] L. Wang, P. Tian, J. Bai: China Concrete and Cement Products Vol.5 (2008), p. 7

[4] Y. Shang: China Building Materials Vol. 3 (1994), p. 24

[5] A. Ge, L. Zhou, P. Chi: J. of Yantai Col. of Education Vol.11 (2005), p.16

[6] J. Sun, Y. Zhou: Ready-mixed Concrete Vol.1(2007), p.21

[7] Q. Tan: China Water Transport Vol.8(2008), p. 219

[8] Z. Chen, X. Tang, G. Sun: The Ocean Engineering Vol.26(2008), p.102

[9] A. Liu, J. Wang: China Sci. and Tech. Information Vol.12(2007), p. 280

[10] W. Ding, F. Leng, W. Zhao: Construction Technology Vol.4 (2007), p. 36

[11] M. Zhang, J. Jiang, Z. Feng: J. of Ocean Uni. of Qingdao Vol.23(2003), p.119

Advanced Materials Research Vols. 450-451 (2012) pp 38-41

doi:10.4028/www.scientific.net/AMR.450-451.38

Effects of solvent polarity on the urethane reaction of 1,2-propanediol

Peng Fei YANG

Shandong Provincial Key Laboratory of Fine Chemicals, Shandong Polytechnic University, Jinan 250353, P.R.China

ypfyyh@gmail.com

Keywords: Isocyanate, Polyurethane, Kinetics, Solvent polarity

Abstract. The urethane reaction kinetics of 1,2-propanediol with phenyl isocyanate are investigated in different solvents, such as xylene, toluene and dimethylformamide. *In-situ* FT-IR is used to monitor the reaction to work out rate constant. It showsthat the urethane reaction has been found to be a second order reaction, solvents largely affects reaction rates. The reaction is largely accelerated in polar solvents, following the order of dimethylformamide > toluene > xylene. Further more, when dimethylformamide is used as solvent, the rate constants are different between initial stage and final stage, which belongs to different hydroxyls in 1,2-propanediol. However, when toluene or xylene is used as solvent, the rate constant is the same. That is, there is no reactivity difference for hydroxyls in 1,2-propanediol.

Introduction

Polyurethanes (PUs) are a very large and varied family of extraordinarily versatile and useful engineering materials. The urethane reactions of alcohols with isocyanates have been widely investigated since Otto Bayer developed the synthetic route of polyurethane [1]. In addition to focus on its application, kinetics of the reaction has been studied all the time [2-4]. There are several factors affecting the urethane reaction rate. As far as the effect of solvent is concerned, it has been reported that the polarity of solvents greatly affected the reaction of alcohols with isocyanates, and the reaction rate falls down with the increase of solvent polarity in the absence of catalyst [5]. However, as far as diol is concerned, little attention is focused on the effects of solvent polarity, such as reaction kinetics of 1,2-propanediol.

1,2-Propanediol is a typical asymmetrical diol, which has been extensively used in polyurethane industry [6]. In order to make clear the effects of polarity, 1,2-propanediol is used to react with phenyl isocyanate in different solvents. React IR is used to monitor the reaction process so as to work out rate constants.

Experimental parts

Materials and instruments. Phenyl isocyanate and 1,2-propanediol were purchased from Sigma Aldrich and used as received. Xylene, toluene and dimethylformamide were purchased from Sinopharm Chemical Reagent Co. and purified by vacuum distillation in the presence of calcium hydroxide.

In-situ FT-IR spectrometer, React IR IC10, was manufactured by Mettler Toledo.

Synthesis and characterization. Clean and dry air was flowed into the instrument continuously until the absorbance of all impurities was constant. Then, the background spectra were recorded. After that, 1,2-propanediol (0.105 g) and solvent (7.00 mL) were poured into the flask and heated to the preset temperature under a nitrogen atmosphere. To this was added the stoichiometric amount of phenyl isocyanate (0.3 mL) when the temperature reached 70 ºC. Thus, the reaction began. Data were collected every half a minute until the reaction was terminated. Resolution was 8 cm^{-1} and scan region was 4000~650 cm^{-1}.

Results and discussion

3D *in-situ* FT-IR spectra. The three-dimensional FT-IR spectra of phenyl isocyanate – 1,2-propanediol reaction is shown in Fig. 1 (2473~2182 cm^{-1}, 70ºC). The absorption at 2273 cm^{-1} proves to be very useful to monitor the reaction, and its decrease in intensity is able to indicate the conversion of isocyanate groups.

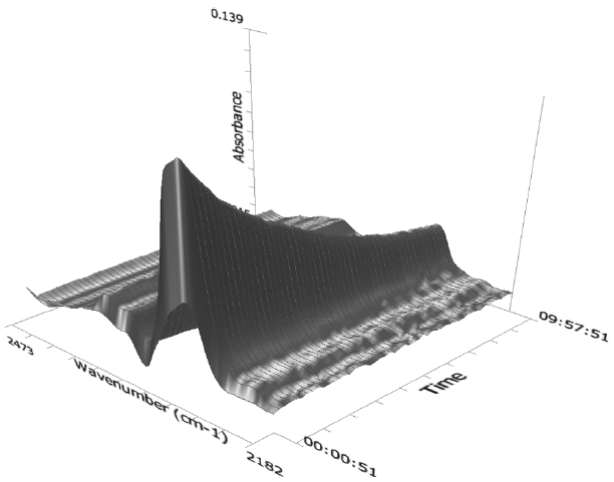

Fig. 1. 3D FT-IR spectra of phenyl isocyanate – 1,2-propanediol reaction

In our former article, it have been reported that Beer's Law (Eq. (1)) seems correct only when the concentration of –NCO is lower than 0.4 $mol \cdot L^{-1}$ [7]. That is, the concentration of IPDI must be less than 0.4 $mol \cdot L^{-1}$ in all kinetic studies.

$$A = k_0 \cdot C \tag{1}$$

In order to obtain the kinetic constants, it is assumed that there is no side reaction. The concentration ($C_{\text{-NCO}}$) can be calculated from absorbance ($A_{\text{-NCO}}$) according to Eq. (1). Assuming it is a second-order process [8], we can use the nth-order approach to model the reaction kinetics (Eq. (2)) when the stoichiometric ratio is used.

$$\frac{1}{A} = \frac{1}{k_0 \cdot C} = k \cdot t + b \tag{2}$$

where k is the apparent rate constant. The value of k can be obtained by adjusting the kinetic model to the experimental results by integrating Eq. (2) with a linear curve fit.

The urethane reaction in dimethylformamide. The urethane reaction of 1,2-propanediol with isocyanate is carried on at 70ºC with dimethylformamide as solvent. Collected data are treated with second-order reaction kinetics and the relationship between $1/A$ and t is shown in Fig. 2.

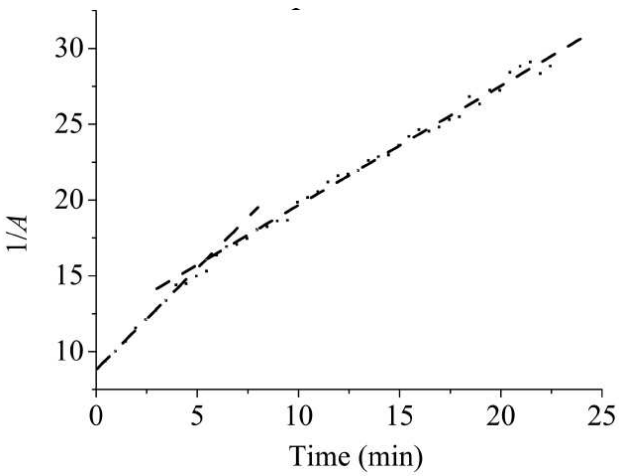

Fig. 2. The relationship between $1/A$ and t with dimethylformamide as solvent

1,2-propanediol have two different hydroxyl groups, a primary hydroxyl and a secondary hydroxyl, which lead to different urethane reaction rate. After carefully examining the reaction, we find that different hydroxyl groups in 1,2-propanediol behave difference reactivity when dimethylformamide is used as catalyst. When reacting with phenyl isocyanate, the rate constant of the primary hydroxyl group (k_1) is 1.34 $L \cdot mol^{-1} \cdot min^{-1}$, and that of the secondary hydroxyl group (k_2) is 7.87×10^{-1} $L \cdot mol^{-1} \cdot min^{-1}$. The reactivity difference, namely, the value of k_1/k_2, is 1.70.

The urethane reaction in toluene. The urethane reaction of 1,2-propanediol with isocyanate is carried on at 70ºC with toluene as solvent. Collected data are treated with second-order reaction kinetics and the relationship between $1/A$ and t is shown in Fig. 3.

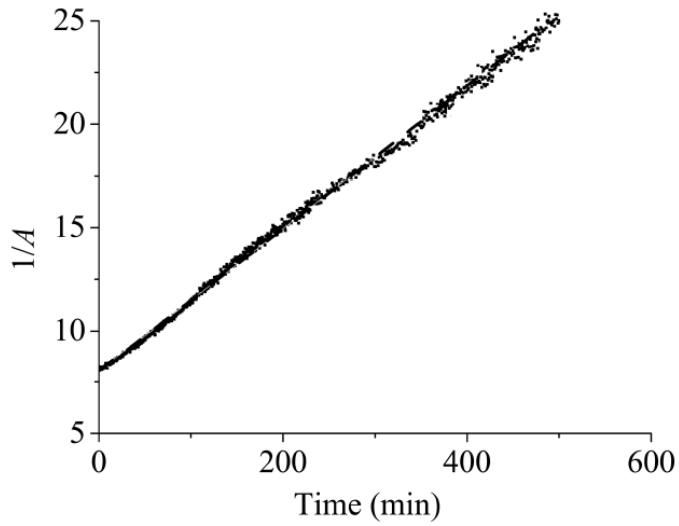

Fig.3. The relationship between $1/A$ and t with toluene as solvent

It is very surprising that there is no reactivity difference between the different hydroxyl groups in 1,2-propanediol. The rate constant of the primary and secondary hydroxyl group is the same. It value is 3.46×10^{-2} $L \cdot mol^{-1} \cdot min^{-1}$.

The urethane reaction in xylene. The urethane reaction of 1,2-propanediol with isocyanate is carried on at 70ºC with xylene as solvent. Collected data are treated with second-order reaction kinetics and the relationship between $1/A$ and t is shown in Fig. 4.

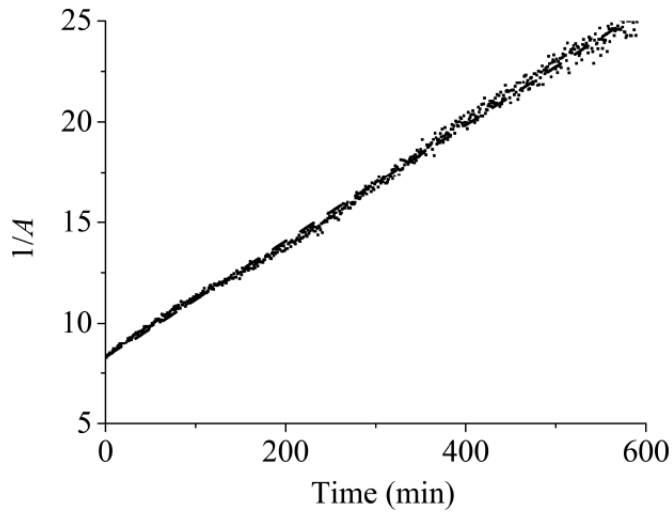

Fig.4. The relationship between $1/A$ and t with xylene as solvent

The situation of xylene is very similar to that of toluene. The rate constant of the primary and secondary hydroxyl group is also the same. It value is 2.89×10^{-2} $L \cdot mol^{-1} \cdot min^{-1}$.

Comparison of rate constants in different solvents. Dimroth–Reichardt parameter, $E_T(30)$, is an official measure of the ionizing power (loosely polarity) of a solvent [9]. It is based on the long-wavelength UV/Vis charge-transfer absorption band of the negatively solvatochromic pyridinium N-phenolate betaine dyes [10]. The $E_T(30)$ values for dimethylformamide, toluene and xylene can be obtained from reference, which are 0.386, 0.099 and 0.074, respectively. It is obvious that the reaction rate varied greatly in different polar solvents. The order is that: dimethylformamide > toluene > xylene, which is the same order as the $E_T(30)$ values (0.386 > 0.099 > 0.074).

Conclusions

In-situ FT-IR is used to monitor the urethane reaction of 1,2-propanediol with phenyl isocyanate. Three different solvents are used, which are dimethylformamide, toluene and xylene. Rate constants are worked out, which are 1.34 $L\cdot mol^{-1}\cdot min^{-1}(k_1)$ and 7.87×10^{-1} $L\cdot mol^{-1}\cdot min^{-1}(k_2)$ for dimethylformamide, 3.46×10^{-2} $L\cdot mol^{-1}\cdot min^{-1}$ for toluene, 2.89×10^{-2} $L\cdot mol^{-1}\cdot min^{-1}$ for xylene, respectively. It is shown that the urethane reaction is a second order reaction. Because there are two different hydroxyl groups in 1,2-propanediol molecule, rate constant in dimethylformamide is different between initial stage and final stage. However, when toluene or xylene is used as solvent, there is no reactivity difference for hydroxyls in 1,2-propanediol. Furthermore, the reaction rate in different solvents follow the order: dimethylformamide > toluene > xylene, which is the same order as the $E_T(30)$ values.

References

[1] P. Król. Progress in Materials Science Vol. 52 (2007) p. 915
[2] S.G. Entelis and O.V. Nesterov. Russian Chemical Reviews Vol. 35 (1966) p. 917
[3] A.A. Caraculacu and S. Coseri. Progress in Polymer Science Vol. 26 (2001) p. 799
[4] M. Pinteala, V. Epure, V. Harabagiu, B.C. Simionescu and S. Schlick. Macromolecules Vol. 37 (2004) p. 4623
[5] A. S. Nasar, A. Raghavan and V. S. Kumar. Journal of Macromolecular Science: Pure and Applied Chemistry Vol. 42 (2005) p. 309
[6] D.K. Chattopadhyay and D.C. Webster. Progress in Polymer Science Vol. 34 (2009) p. 1068
[7] P. F. Yang, Y.D. Han, T.D. Li, J.Y. Li. Journal of Applied Polymer Science Vol. 123 (2012) p. 580
[8] S. Ajithkumar, S.S. Kansara and N.K. Patel. European Polymer Journal Vol. 34 (1998) p. 1273
[9] C. Reichardt. *Solvents and Solvent Effects in Organic Chemistry (Third, Updated and Enlarged Edition)* (Wiley-VCH, Marburg 2003)
[10] C. Reichardt. Chemical Reviews Vol. 94 (1994) p. 2319

Advanced Materials Research Vols. 450-451 (2012) pp 42-45

doi:10.4028/www.scientific.net/AMR.450-451.42

Effects of Al_2O_3 on the Structure and Properties of Calcium-Magnesium-Silicate Glass Fiber

Hao Liu [a], Xitang Wang [b], Zhoufu Wang [c] and Baoguo Zhang [d]

The Key State Laboratory Breeding Base of Refractories and Ceramics, Wuhan University of Science and Technology, Wuhan 430081, China

[a] wustlh@163.com, [b] whwxt-888@163.com, [c] whwzf@ton.com, [d] zbg0004@163.com

Keywords: Glass fiber, Crystallization, Dissolution.

Abstract. Calcium-magnesium-silicate glass fiber is a kind of candidate materials for aluminosilicate ceramic fiber in high temperature resistant field. However, the large thermal shrinkage limits its rapid development and industrial application in high temperature insulation field. It has been known that the shrinkage under high temperatures is mainly affected by the structure and crystallization mechanisms of glass fibers. Thus, Al_2O_3 was chosen as additive in the chemical composition of glass fiber to investigate the glassy network structure, crystallization and dissolution properties of calcium-magnesium-silicate glass fiber by DTA, XRD and ICP-AES techniques. The results show that with the addition of Al_2O_3, the glassy network structure was strengthened and the precipitation of crystals was inhibited for heat-treated fibers. As for the dissolution properties in physiological fluids, though the weight losses, changes of pH values and leached ions concentration lowered slightly with the addition of Al_2O_3 for the intensified network structure, fibers still present high dissolution rates.

Introduction

It has been known that the dust particles of aluminosilicate refractory ceramic fiber may cause serious health effects such as cancer or fibrosis if inhaled in human respiratory system [1]. Thus, there has been increasing interest in looking for new system ceramic /glass fibers and the health effect of inhaled fibrous materials [2]. These new system fibers have been designed to be used as thermal insulating materials in high temperature as in the way that some mineral fibers and aluminosilicate refractory ceramic fiber are used at present. As candidate materials for traditional ceramic fiber, low biopersistence in simulated body /lung fluid is needed for the mentioned new fibers, which is designed to be composed of SiO_2 and alkaline earth oxides (MgO, CaO, BaO), such as CaO-MgO-SiO_2 glass fiber.

CaO-MgO-SiO_2 glass fiber is designed to have high dissolution rate in simulated body fluid, and high serving temperature (~1100˚C). However, the large shrinkage under high temperature (>800˚C) restricts the application and lower the serving life of fibers. It has been known that the thermal shrinkage is mainly from the crystallization of fibers under high temperatures. Thus, to inhibit the crystallization of fibers may be a useful way to decrease the thermal shrinkage. As for glass materials, alkaline oxide, alkaline-earth oxide, Al_2O_3 and rare earth oxide have been added into the composition to adjust the glass network structure and properties [3-5]. Similar methods may be useful for the improvement of structure and performances of fibers.

This study presents the results of glass structure, crystallization and dissolution performances of the mentioned glass fiber added with Al_2O_3.

Experimental

The major starting materials are wollastonite, silica and Al_2O_3 (analytical reagent). The main chemical compositions of fiber samples are listed in Table 1. After thoroughly mixed, the weighed batch materials were melted in a graphite crucible at 1600-1800˚C for 30-50min. Then the melts were sprayed into fibers by compressed air under 0.3-0.5 MPa.

Table 1 Main compositions (wt %) and characteristic temperatures of fibers.

No.	*CaO*	*MgO*	*SiO_2*	*Al_2O_3*	*T_g(˚C)*	*T_c(˚C)*	*T_c-T_g(˚C)*
A0	30.6	6.9	61.0	-	747	893	146
A1	30.3	6.8	60.4	1	752	935	183
A2	30.1	6.6	59.8	2	749	905	156

Glass transition temperature (Tg), crystallization exothermal temperature (Tc) of fiber samples were measured by a DTA (STA449/6/G Netzsch, Germany), operating at 15˚C/min heating rate from room temperature to 1000˚C in air.

The X-ray diffraction (XRD) spectra of the fine powdered fibers were recorded with an X'portpro diffractometer. The Cu-Kα radiation (λ=0.15405μm) was used at 50kV and 40mA. X-ray patterns were gathered in the range 10-80° 2θ with a step size of 0.03° and a step time of 7s.

The dissolution of the fibers was investigated at 37˚C in simulated lung fluid, e.g., Gamble solution, with the initial pH 7.4 [6]. The grinded fragments of fibers about 20-100μm long were laid in the teflon reactor. The weight of the fibers was 2 ± 0.0001g and the volume of the solution was 1000ml. The immersing runs for fibers were performed from 0-72h. After each run, the fibers were removed from the solution, then rinsed with deionized water and dried at 37˚C for 12h in an oven before weighing. Changes of ions concentration in solution were determined by an inductively coupled plasma atomic emission spectroscopic (ICP-AES) analysis.

Results and discussion

Fig.1 shows the DTA curve of fiber A0, and Table 1 presents the characteristic temperatures (T_g and T_c). It can be seen that the addition of Al_2O_3 in fibers leads to the increase in T_c and the range between T_g and T_c. Besides, T_c and range between T_g and T_c of fibers decreased with the addition of Al_2O_3. The temperature of T_c and the shape of exothermic peak shape indicate the crystallization behavior of glassy materials, and the range between T_g and T_c shows the ability to be formed into glassy materials for the studied compositions. Thus, the changes of the characteristic temperatures for Al_2O_3 doped samples present the differences of glass network and crystallization process of fibers. With low content of Al_2O_3 (fiber A1), Al^{3+} is surrounded by O^{2-} forming Al-O tetrahedron and intensifying the silicate network [7]. However, the radius of Al^{3+} is larger than that of Si^{4+}, accordingly, the volume of Al-O tetrahedron is larger than that of Si-O tetrahedron. Thus, low content of Al^{3+} in glassy materials could amend the defects of network, and more content of Al^{3+} would result in large content of Al-O tetrahedron and distortion of network structure.

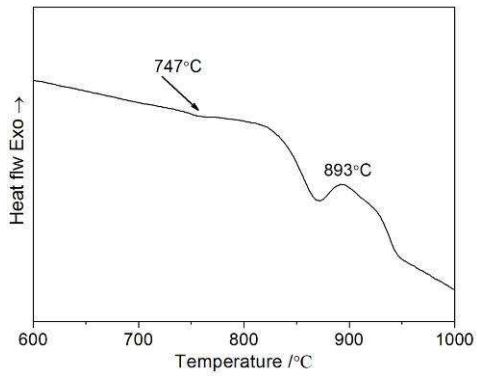

Fig.1 DTA curve of fiber A0.

Fig.2 shows the XRD patterns of fiber samples heat-treated at 800˚C for 2h. After treated for 2h, wollastonite precipitated as major crystalline phase in fiber A0, and tiny akermanite could also be observed. In fiber A1 and A2, with the addition of Al_2O_3, not any crystalline phases could be observed from the pattern, which means the addition of Al_2O_3 could inhibit the precipitation of silicate crystals in fibers at 800˚C. As for samples treated at 900˚C in Fig.3, diopside also precipitated in fiber A0.

With the addition of Al_2O_3, the types of precipitated crystalline phases keep the same with A0, only the diffraction intensity of wollastonite decreases compared with A0. Besides, the diffraction intensity of crystalline phases in fiber A2 is larger than A1.

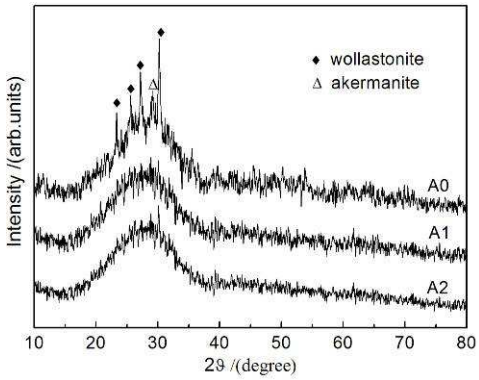

Fig.2 XRD patterns of treated fibers (800˚C for 2h).

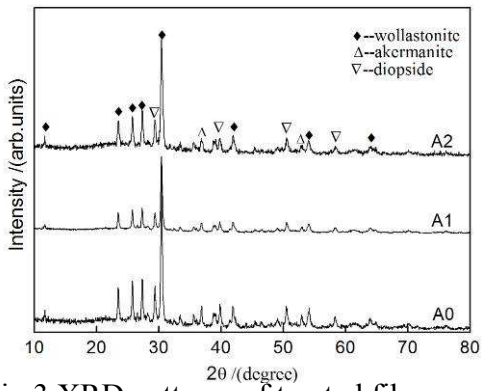

Fig.3 XRD patterns of treated fibers (900˚C for 2h).

During the dissolution process, Ca^{2+} and Mg^{2+} were firstly leached out from the fiber surface, resulting in the accretion of OH^- concentration and rapid increase of pH value of the solution. As shown in Fig.4, the changes of pH value for the three samples are similar, though the increment of pH value of fiber A0 is larger than samples with Al_2O_3.

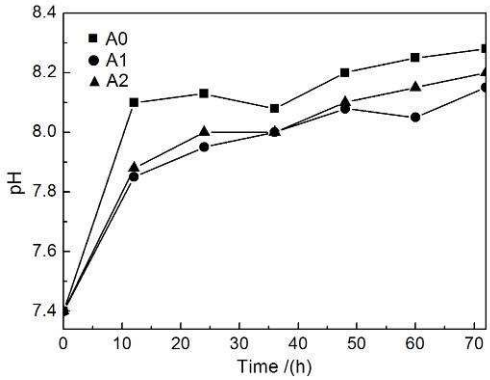

Fig.4 Changes of pH of solution for different durations.

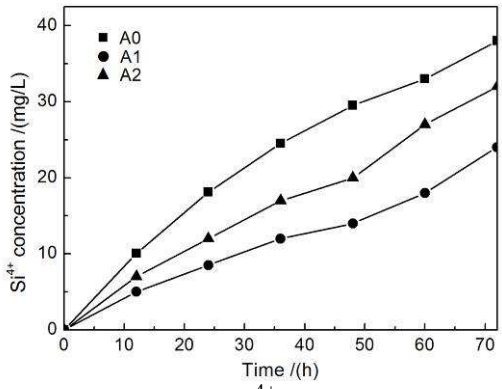

Fig.5 Changes of Si^{4+} ions concentration in Gamble solution.

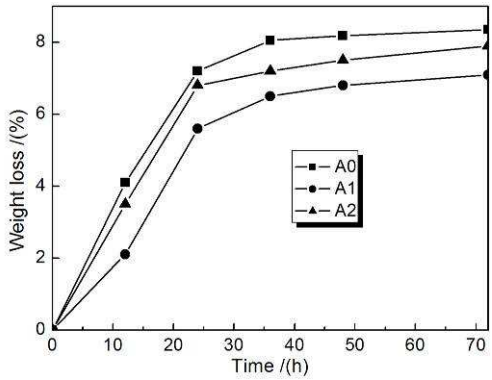

Fig. 6 Weight loss of immersed fiber samples for different durations.

The dissolution of fibers starts from the leaching of alkaline earth ions on the fiber surface in the solution, resulting in the rupture of silicate network and leaching of Si^{4+} into the solution [8]. Part of the leached Si^{4+}, Ca^{2+} and Mg^{2+} could react and generate alkaline earth silicate hydration layer on the fiber surface, which would be washed off by the fluid flow of the solution. Thus, the concentrations of major ions in the solution increased gradually (Fig.5). The change of weight loss (Fig.6), which is an important parameter to evaluate the solubility performances of bio-soluble materials [9], is similar with that of pH values. That is, the weight loss increased rapidly at the initial 24h of the dissolution process, and then tended into a gradual increasing process. However, the dissolution rates (changes of

pH value, weight loss and ions concentration) of fibers with Al_2O_3 are lower than fiber A0, and that of fiber A2 is larger than A1, which means that the addition of lower content of Al_2O_3 intensify the silicate network of glass fibers, and more content of Al_2O_3 weakens the effects on the strengthening of network. The reasons are similar with the above results analyzed from crystallization behavior of fibers.

Conclusions

The addition of lower content of Al_2O_3 in CaO-MgO-SiO_2 glass fiber could intensify the glassy network and increases the characteristic temperatures of fibers. And more content of Al_2O_3 (more than 2%) would weaken the mentioned effects. As for the dissolution performances, changes of pH value, weight loss and ions concentration were lowered for the intensified silicate network with the addition of Al_2O_3.

Acknowledgements

This work was financially supported by the National Natural Science Foundation of China (51004080), the Opening Fund of the Key State Laboratory Breeding Base of Refractories and Ceramics (Wuhan University of Science and Technology, G201004).

References

[1] International Agency for Research on Cancer (IARC). Monographs on The Evaluation of Carcinogenic Risk to Humans: Man-made Vitreous Fibres. Lyon, France, Vol.81(2002), p.57

[2] H. Liu, X.T. Wang, Z.F. Wang and B.G. Zhang: Journal of Wuhan University of Science and Technology, Vol.32 (2009), p.170 (in Chinese)

[3] F.T. Wallenberger, R.J. Hichs and A.T. Bierhals: J. Non-Cryst. Solids, Vol.349(2004), p.377

[4] J.J. Shyu and C.S. Hwang: J. Mater. Sci., Vol.31(1996), p.2631

[5] H. Liu, X.T. Wang, Z.F. Wang and B.G. Zhang: Advan. Mater. Res., Vol.295-297(2011), p.406

[6] R.M. Potter: Glastech. Ber., Vol.64(1991), p.16

[7] S. Sen and J.F.Stebbin: J. Non-cryst. Solids, Vol.188(1995), p.1

[8] P.M. Dove and D.A. Crerara: Geochim. Cosmochim. Acta, Vol.54(1990), p.955

[9] Manupriya, K.S. Thind , K. Singh, V. Kumar, G. Sharma, D.P. Singh and D. Singh: J. Phys. Chem. Solids, Vol.70(2009), p.1137

Advanced Materials Research Vols. 450-451 (2012) pp 46-55
© (2012) Trans Tech Publications, Switzerland
doi:10.4028/www.scientific.net/AMR.450-451.46

A Class of Stochastic Control Problem Governed by a Poisson Process

Shaolin Tian[1a], Jichun Li[2b] and Kunhui Liu [3c]

[1]College of Sciences, Beijing Jiaotong University, Beijing 100044, China

[2]Department of Mathematical Sciences, University of Nevada Las Vegas, NV 89154-4020, USA

[3]College of Sciences, Beijing Jiaotong University, Beijing 100044, China

[a]E-mail: tsl1225@163.com.

[b]E-mail:jichun@unlv.nevada.edu.

[c]E-mail: khliu@bjtu.edu.cn.

Keywords: Impulse contro, Variational inequality, Generalized Ito formula, Poisson process, Optimal stopping

Abstract. In this paper, we examine an optimal impulse control problem of stochastic system, whose state follows a Brownian motion. Here we want to maximum the objective function. The main feature of our model is that the controlled state process includes an impulse control governed by a Poisson process. In other words, the set of possible intervention times are discrete, random and determined by the signal process. Here we not only present a theorem giving a sufficient condition on the existence of an optimal control and its corresponding objective function, but also provide an explicit solution obtained under some simplified conditions.

Introduction

In this paper, we discuss a stochastic control problem with random intervention times. The controlled state process includes an impulse control governed by a Poisson process. The state evolution is modeled as follows:

$$\mathrm{X_t} = x + \mu t + \sigma W_t - \xi_t \tag{1.1}$$

with the initial state

$$X(0) = x \tag{1.2}$$

where $\mu \geq 0$, $\sigma \geq 0$, $x \geq 0$, and $W = \{W(t) : t \geq 0\}$ is a standard Brownian motion defined on some probability space $(\Omega, F, \{F_t\}, P)$ with filtration $\{F_t\}$ satisfying the usual conditions: right-continuity and completion by P-negligible sets. Again, the class of admissible controls, denoted by Π, consists of those left-continuous processes $\xi = \{\zeta_\mathrm{t}; t \geq 0\}$ that have the following representation:

$$\zeta_t = \int_{[0,t)} \theta_s dN_s \quad \text{and such that} \quad X(t) \geq 0 \tag{1.3}$$

Where $N = \{N_t; t \geq 0\}$ is an $\{F_t\}$-adapted Poisson process with intensity λ, and $\theta = \{\theta_t t \geq 0\}$ is assumed to be non-negative and $\{F_t\}$-progressively measurable. In other words, controls can only be exerted at the arrival times of Poisson process *N*. The controlled process $X(t)$ determined by Eq.(1.1) seems to be a singular control process. In fact, since N is an impulse control, $X(t)$ is an impulse state process. The solution of Eq.(1.1) is unique (see [1]).

Throughout this paper, we impose the following assumption:

Assumption 1.1. The Brownian motion $W(t)$ and the Poisson process N_t are independent.

Also we define stopping time as

$$\tau_0 = \inf\{\mathrm{t} \geq 0 \colon X(t) = 0\} \tag{1.4}$$

and the objective function from present to stopping time as

$$V_\xi(t) = E\int_0^{\tau_0} e^{-rt}(X_t dt + c d\xi_t), \tag{1.5}$$

where c > 0 is an arbitrary positive constant, and the constant r > 0 represents the discounted factor.

Furthermore, we assume that

$$V_\xi(t) = E\int_0^{\tau_0} e^{-rt}(X_t dt + c d\xi_t) \text{ is integrable for any admissible control } \xi \in \Pi. \tag{1.6}$$

One of the main objectives of this paper is to solve:

Problem 1.1. Find an optimal control $\xi^* = \{\xi_t^* : t \geq 0\} \in \Pi$ such that

$$V(x) = V_{\xi^*}(x) = \sup_{\xi \in \Pi} V_\xi(x) \tag{1.7}$$

The function V (x) given by (1.7) is called the optimal objective function.

There exist many papers in the field of singular stochastic and impulse stochastic control. These control problems have found applications in many areas such as engineering, economics, finance and biocenology, etc. The models of singular stochastic control were initiated in [2], and more extensions can be found in [2]-[13]. One major attraction of this formulation lies in the possibility of obtaining explicit solutions, especially when the time horizon is infinite. The optimal strategies in such occasions are often singular with respect to the Lebesgue measure. The models of impulse stochastic control have also been studied intensively in last three decades, see [14]-[18]. The control policies were adjusted only at times which are multiples of some fixed positive number. The decision makers are allowed to choose a sequence of stopping times (intervention times) $\{\tau_1, \tau_2, \ldots\}$, and a sequence of impulse controls $\{\xi_1, \xi_2, \ldots\}$ to be imposed upon the system at $\{\tau_1, \tau_2, \ldots\}$ respectively. Explicit solutions are possible for simple causes.

One main feature of this model is that the control policy is essentially discrete, in the sense that the control can only be exerted at times when the Poisson process N has a jump. In other words, controls can only be adjusted at the discrete random times $0 < T_1 < T_2 < T_3 < \ldots$, where $\{T_1, T_2 - T_1, T_3 - T_2, \ldots\}$ are independent and identically distributed exponential random variables with rate λ. The other main feature is that the possible intervention times are completely determined by the exogenous, uncontrolled Poisson process N: In other words, the decision maker cannot intervene in the system freely. In order to impose controls, the decision maker has to rely on the Poisson process to give him/her a certain signal (in this case, the jumps).

Our formulation allows us to obtain explicit solutions for some models with stopping time, while the underlying control strategies are kept discrete. The difference from the usual impulse control problems is that the intervention times are no longer totally free to the decision maker - they are essentially determined by the exogenous signal process (the Poisson process N). To our best knowledge, such constrains on the intervention time were considered in [19]. In that case, the state process is an ideal situation that doesn't include drift parameters. Therefore, in this paper, we discuss a similar model again. Here we introduce the drift parameter μ into the controlled state and the stopping time into its objective structure. We extend the structure of the objective function. Then we prove the existence of optimal control and characterize the explicit forms for the optimal control. More specifically, not only the existence of optimal control is fully proved, but also the explicit forms of optimal control is characterized.

This paper is organized as follows. In Sect. 2, we prove a theorem which gives the criterion for the optimal objective function. In Sect. 3, we solve the variation equations and obtain an explicit forms of optimal control and corresponding maximal objective function. We conclude our paper in Sect. 4.

A Verification Theorem

In this section, we will provide a theorem giving a sufficient condition for the existence of the optimal ojective function. Before analyzing this any further, we state the following auxiliary verification lemma.

Lemma 2.1 For any given constant c > 0, suppose that there exists a positive constant m and a function $v(x) \in C^2([0,\infty))$ (i.e., v(x) has continuous derivatives of order up to 2) such that

$$v''(x) \leq 0, \quad \forall x \geq 0, \tag{2.1}$$

And

$$v'(m) = c \tag{2.2}$$

Denote $\theta^* = \arg\max_{\theta}\{v(x-\theta) - v(x) + c\theta : 0 \le \theta \le x\}$, then we have

$$\theta^* = \begin{cases} 0, & 0 \le x \le m, \\ x - m, & x \ge m. \end{cases} \tag{2.3}$$

Proof. Differentiation of $v(x-\theta) + c\theta$ with respect to θ shows that

$$(v(x-\theta) + c\theta)' = -v'(x-\theta) + c = \int_{x-\theta}^{m} v''(y)dy .$$

When x $\ge$ m, using (2.1) and (2.2) in the above identity, we can easily see that

$$-v'(x-\theta) + c \le 0, \qquad \theta \ge x - m$$

$$-v'(x-\theta) + c \ge 0 \qquad 0 \le \theta \le x - m$$

Thus, $v(x-\theta) - v(x) + c\theta$ attains its maximum at $x - m$.

On the other hand, for $x \in [0, m]$, we have $0 \le x - \theta \le m$. Hence by (2.1) and (2.2), we know $-v'(x-\theta) + c \le 0$, so $v(x-\theta) - v(x) + c\theta$ is decreasing with respect to θ. Therefore, $v(x-\theta) - v(x) + c\theta$ attains its maximum at $\theta = 0$, which concludes the proof.

Theorem 2.1 Assume that v(x) satisfy all the conditions of Lemma 2.1 and

$$v(0) = 0 \tag{2.4}$$

$$v'(x) \in (0, c], \quad \forall x \ge m \tag{2.5}$$

and

$$\max_{0 \le \theta \le x}\left\{\frac{\sigma^2}{2}v''(x) + \mu v'(x) - (r+\lambda)v(x) + x + \lambda(v(x-\theta) + c\theta)\right\} \le 0 \tag{2.6}$$

Then we have

$$v(x) \ge V(x), \quad \forall x \ge 0 \tag{2.7}$$

Furthermore, if v(x) satisfies

$$\frac{\sigma^2}{2}v''(x) + \mu v'(x) - (r+\lambda)v(x) + x + \lambda(v(m) - c(x-m)) = 0, \quad x > m, \tag{2.8}$$

and

$$\frac{\sigma^2}{2}v''(x) + \mu v'(x) - rv(x) + x = 0, \quad 0 \le x \le m, \tag{2.9}$$

then there exists ξ^* such that

$$v(x) = V_{\xi^*}(x),$$

i.e., ξ^* is an optimal control, and v(x) is the corresponding objective function.

Proof. For any T > 0, applying the Generalized Ito formula ([20], Chapter 8) to the process $e^{-rt}v(X_t) : t \ge 0$, we obtain

$$\begin{aligned} e^{-r(T\wedge\tau_0)}v(X(T\wedge\tau_0)) - v(x) &= \int_0^{T\wedge\tau_0} e^{-rt}\left\{\frac{\sigma^2}{2}v''(X(t)) + \mu v'(X(t)) - rv(X(t))\right\}dt \\ &+ \int_0^{T\wedge\tau_0} e^{-rt}\sigma v'(X(t))dW(t) + \sum_{0\le t\le T\wedge\tau_0}[v(X(t) - \Delta\xi_t) - v(X(t))], \end{aligned} \tag{2.10}$$

where $\Delta\xi_t = X(t) - X(t+)$) and = $T \wedge \tau_0 = \min\{T, \tau_0\}$, from which we have

$$\begin{aligned} v(x) = e^{-r(T\wedge\tau_0)}v(X(T\wedge\tau_0)) &- \int_0^{T\wedge\tau_0} e^{-rt}\left\{\frac{\sigma^2}{2}v''(X(t)) + \mu v'(X(t)) - rv(X(t))\right\}dt \\ &- \int_0^{T\wedge\tau_0} e^{-rt}\sigma v'(X(t))dW(t) - \sum_{0\le t\le T\wedge\tau_0}[v(X(t) - \Delta\xi_t) - v(X(t))], \end{aligned} \tag{2.11}$$

Note that (2.6) can be written as

$$\left[\frac{\sigma^2}{2}v''(x)+\mu v'(x)-rv(x)\right]+\max_{0\le\theta\le x}\{\lambda v(x-\theta)-v(x)+c\theta\}+x\le 0,$$

or

$$-\left[\frac{\sigma^2}{2}v''(x)+\mu v'(x)-rv(x)\right]\ge\max_{0\le\theta\le x}\{\lambda(v(x-\theta)-v(x)+c\theta)\}+x\,.$$

Applying Lemma 2.1, we have

$$g(x)\equiv\max_{0\le\theta\le x}\{v(x-\theta)-v(x)+c\theta\}=0,\qquad 0\le x\le m,$$

$$g(x)\equiv\max_{0\le\theta\le x}\{v(x-\theta)-v(x)+c\theta\}=v(m)-v(x)+c(x-m),\qquad x\ge m,\tag{2.12}$$

Noting that $\Delta\xi_t>0$ only if there is a Poisson jump at time t, hence we have

$$v(X(t)-\Delta\xi_t)-v(X(t))+c\Delta\xi_t\le g(X(t))dN_t\,.\tag{2.13}$$

Using the identity $\int_0^{T\wedge\tau_0}e^{-rt}d\xi_t=\sum_{0\le t\le T\wedge\tau_0}e^{-rt}\Delta\xi_t$ and the fact v(x) $\ge$ 0, then combining (2.12), (2.13) with (2.11), we obtain

$$\begin{aligned}
v(x)&\ge e^{-r(T\wedge\tau_0)}v(X(T\wedge\tau_0))+\int_0^{T\wedge\tau_0}e^{-rt}\left[\lambda g(X(t))+X(t)\right]dt\\
&\quad-\sum_{0\le t\le T\wedge\tau_0}e^{-rt}(v(X(t)-\Delta\xi_t)-v(X(t))+c\Delta\xi_t)\\
&\quad-\int_0^{T\wedge\tau_0}e^{-rt}\sigma v'(X(t))dW(t)+c\int_0^{T\wedge\tau_0}e^{-rt}d\xi_t\\
&\ge e^{-r(T\wedge\tau_0)}v(X(T\wedge\tau_0))+\int_0^{T\wedge\tau_0}e^{-rt}X(t)dt\\
&\quad-\int_0^{T\wedge\tau_0}e^{-rt}g(X(t))d\hat{N}t-\int_0^{T\wedge\tau_0}e^{-rt}\sigma v'(X(t))dW(t)+c\int_0^{T\wedge\tau_0}e^{-rt}d\xi_t\\
&\ge-\int_0^{T\wedge\tau_0}e^{-rt}g(X(t))d\hat{N}t-\int_0^{T\wedge\tau_0}e^{-rt}\sigma v'(X(t))dW(t)\\
&\quad+c\int_0^{T\wedge\tau_0}e^{-rt}d\xi_t+\int_0^{T\wedge\tau_0}e^{-rt}X(t)dt,
\end{aligned}\tag{2.14}$$

where $\hat{N}_t=\{N_t-\lambda t{:}t\ge 0\}$ is the Compensated Poisson process. Obviously, $\hat{N}$ is a continuous-time martingale (see[21] pp.12), hence it is a local martingale too.

Denote

$$Z_T=\int_0^{T\wedge\tau_0}e^{-rt}g(X(t))d\hat{N}(t),\qquad M_T=\int_0^{T\wedge\tau_0}e^{-rt}\sigma v'(X(t))dW(t)\,.$$

In light of the continuity of g(x), we know that Z_T is a local martingale (e.g., [22],[23]), and consequently -(Z_T + M_T) is a local martingale too. Hence there exists a stopping sequences $\tau_n'\uparrow\infty$ a.s.(n $\uparrow\infty$), such that $-(Z_{T\wedge\tau_n'}+M_{T\wedge\tau_n'})$ is a martingale with initial value 0, in particular

$$E\left[-(Z_{T\wedge\tau_n'}+M_{T\wedge\tau_n'})\right]=0\,.$$

Thus, from (2.14) we know that $-(Z_{T\wedge\tau_n'}+M_{T\wedge\tau_n'})\le$ v(x). Applying Fatou Lemma, we have

$$\begin{aligned}
E\left[-(Z_{T\wedge\tau_n'}+M_{T\wedge\tau_n'})\right]&=E\limsup_{n\to\infty}\left[-(Z_{T\wedge\tau_n'}+M_{T\wedge\tau_n'})\right]\\
&\ge\limsup_{n\to\infty}\left[-(Z_{T\wedge\tau_n'}+M_{T\wedge\tau_n'})\right]=0
\end{aligned}$$

Therefore, taking expectation on both sides of (2.14), we obtain

$$v(x)\ge E[\int_0^{T\wedge\tau_0}ce^{-rt}d\xi_t+\int_0^{T\wedge\tau_0}e^{-rt}X(t)dt]\tag{2.15}$$

Since Eq. (2.15) is valid for any admissible controls, it has to be true for the optimal one ξ^*.

Therefore, for all $x \in [0,\infty)$, we have that

$$v(x) \geq V_{\xi^*}(x) = V(x) \tag{2.16}$$

It remains to show that there exists an optimal control $\xi^* \in \Pi$ such that $v(x) = V_{\xi^*}(x)$. Let $\xi^* = \{\xi_t^*; t \geq 0\}$, where

$$\xi_t = \int_{[0,t)} \theta_s^* dN_s$$

and

$$\theta_s^* = \begin{cases} 0, & 0 \leq X^*(s) \leq m, \\ X^*(s) - m, & X^*(s) \geq m. \end{cases} \tag{2.17}$$

Here the superscript * represents the relation to optimal control ξ^*. We only need to show that $v(x) \leq V_{\xi^*}(x)$. Actually, it is easy to see that (2.16) is indeed an equality as $\xi = \xi^*$.

Similar to (2.11), we have

$$\begin{aligned} v(x) = e^{-r(T\wedge\tau^*{}_0)} v(X^*(T\wedge\tau_0)) - \int_0^{T\wedge\tau^*{}_0} e^{-rt}\left\{\frac{\sigma^2}{2}v''(X^*(t)) + \mu v'(X^*(t)) - rv(X^*(t))\right\}dt \\ - \int_0^{T\wedge\tau^*{}_0} e^{-rt}\sigma v'(X^*(t))dW(t) - \sum_{0\leq t\leq T\wedge\tau^*{}_0}\left[v(X^*(t) - \Delta\xi^*{}_t) - v(X^*(t))\right], \end{aligned} \tag{2.18}$$

where $\Delta\xi_t^* = X^*(t) - X^*(t+) \geq 0$.

Noting that $\int_0^{T\wedge\tau_0^*} e^{-rt} d\xi_t^* = \sum_{0\leq t\leq T\wedge\tau_0^*} e^{-rt}\Delta\xi_t^*$ and

$$v(X^*(t) - \Delta\xi_t^*) - v(X^*(t)) + c\Delta\xi_t^* = g(X^*(t))dN_t^*,$$

we can rewrite (2.18) as

$$\begin{aligned} v(x) &= e^{-r(T\wedge\tau^*{}_0)} v(X^*(T\wedge\tau^*{}_0)) - \int_0^{T\wedge\tau^*{}_0} e^{-rt}\left\{\frac{\sigma^2}{2}v''(X^*(t)) + \mu v'(X^*(t)) - rv(X^*(t))\right\}dt \\ &\quad + c\int_0^{T\wedge\tau^*{}_0} e^{-rt} d\xi_t^* - \int_0^{T\wedge\tau^*{}_0} e^{-rt}\sigma v'(X^*(t))dW(t) \\ &\quad - \sum_{0\leq t\leq T\wedge\tau^*{}_0} e^{-rt}\left[v(X^*(t) - \Delta\xi^*{}_t) - v(X^*(t)) + c\Delta\xi_t^*\right] \\ &= e^{-r(T\wedge\tau^*{}_0)} v(X^*(T\wedge\tau^*{}_0)) - \int_0^{T\wedge\tau^*{}_0} e^{-rt}\left\{\frac{\sigma^2}{2}v''(X^*(t)) + \mu v'(X^*(t)) - rv(X^*(t))\right\}dt \\ &\quad + c\int_0^{T\wedge\tau^*{}_0} e^{-rt} d\xi_t^* - \int_0^{T\wedge\tau^*{}_0} e^{-rt}\sigma v'(X^*(t))dW(t) - \int_0^{T\wedge\tau_0} e^{-rt} g(X^*(t))dN_t \end{aligned}$$

$$\begin{aligned} &= e^{-r(T\wedge\tau^*{}_0)} v(X^*(T\wedge\tau^*{}_0)) + c\int_0^{T\wedge\tau^*{}_0} e^{-rt} d\xi_t^* \\ &\quad - \int_0^{T\wedge\tau^*{}_0} e^{-rt}\left\{\frac{\sigma^2}{2}v''(X^*(t)) + \mu v'(X^*(t)) - rv(X^*(t)) + \lambda g(X^*(t))\right\}dt \\ &\quad - \int_0^{T\wedge\tau^*{}_0} e^{-rt}\sigma v'(X^*(t))dW(t) - \int_0^{T\wedge\tau_0} e^{-rt} g(X^*(t))dN_t, \end{aligned} \tag{2.19}$$

where $\hat{N}^* = \{N_t - \lambda t : t \geq 0\}$ is the Compensated Poisson process. Obviously $\hat{N}^*$ is a martingale, and it is a local martingale too.

From the definition of g(x), we know

$$g(X^*(t)) = 0 \qquad 0 \le X^*(t) \le m$$
$$g(X^*(t)) = v(m) - v(X^*(t)) + c(X^*(t) - m) \qquad X^*(t) \ge m \tag{2.20}$$

Substituting (2.20) into (2.19), and using (2.8)-(2.9), we have that

$$v(x) = e^{-r(T\wedge\tau^*{}_0)} v(X^*(T\wedge\tau_0^*)) - (Z_T^* + M_T^*) + c\int_0^{T\wedge\tau^*{}_0} e^{-rt} d\xi_t^* + \int_0^{T\wedge\tau^*{}_0} e^{-rt} X^*(t)dt \tag{2.21}$$

where $Z_T^* = \int_0^{T\wedge\tau_0^*} e^{-rt} g(X^*(t))d\hat{N}_t^*$, $M_T^* = \int_0^{T\wedge\tau_0^*} e^{-rt}\sigma v'(X^*(t))dW(t)$ Since $-(Z_T^* + M_T^*)$ is a local martingale, there exists a stopping sequences $\tau_n^{''} \uparrow \infty$ a.s. ($n \uparrow \infty$), such that $-(Z_{T\wedge\tau_n''}^* + M_{T\wedge\tau_n''}^*)$ is a martingale with initial value 0, particularly

$$E\left[-(Z_{T\wedge\tau_n''}^* + M_{T\wedge\tau_n''}^*)\right] = 0.$$

Eq. (2.21) still holds with $T\wedge\tau_n^{''}$ instead of T, i.e.

$$\begin{aligned} v(x) &= e^{-r(T\wedge\tau_n''\wedge\tau_0^*)} v(X^*(T\wedge\tau_n''\wedge\tau_0^*)) - (Z_{T\wedge\tau_n''}^* + M_{T\wedge\tau_n''}^*) \\ &\quad + c\int_0^{T\wedge\tau_n''\wedge\tau_0^*} e^{-rt} d\xi_t^* + \int_0^{T\wedge\tau_n''\wedge\tau_0^*} e^{-rt} X^*(t)dt \end{aligned} \tag{2.22}$$

Therefore, taking expectation on both side of (2.22), we have

$$v(x) = Ee^{-r(T\wedge\tau_n''\wedge\tau_0^*)} v(X^*(T\wedge\tau_n''\wedge\tau_0^*)) + cE\int_0^{T\wedge\tau_n''\wedge\tau_0^*} e^{-rt} d\xi_t^* + E\int_0^{T\wedge\tau_n''\wedge\tau_0^*} e^{-rt} X^*(t)dt \tag{2.23}$$

To complete the proof, below we will discuss two cases.

(i) The case for $\tau_0^* < \infty$.

According to Lebesgue dominated convergence theorem, letting $\tau'' \uparrow \infty$ ($n \to \infty$) and $T \to \infty$, we obtain

$$\begin{aligned} v(x) &= Ee^{-r\tau_0^*} v(X^*(\tau_0^*)) + cE\int_0^{\tau_0^*} e^{-rt} d\xi_t^* + E\int_0^{\tau_0^*} e^{-rt} X^*(t)dt \\ &= Ee^{-r\tau_0^*} v(0) + cE\int_0^{\tau_0^*} e^{-rt} d\xi_t^* + E\int_0^{\tau_0^*} e^{-rt} X^*(t)dt \\ &= cE\int_0^{\tau_0^*} e^{-rt} d\xi_t^* + E\int_0^{\tau_0^*} e^{-rt} X^*(t)dt \end{aligned} \tag{2.24}$$

(ii) The case for $\tau_0^* = \infty$.

When $\tau_0^* = \infty$, (2.23) can be rewritten as

$$v(x) = Ee^{-r(T\wedge\tau_n'')} v(X^*(T\wedge\tau_n'')) + cE\int_0^{T\wedge\tau_n''} e^{-rt} d\xi_t^* + E\int_0^{T\wedge\tau_n''} e^{-rt} X^*(t)dt$$

According to Lebesgue dominated convergence theorem, letting $\tau'' \uparrow \infty$ ($n \to \infty$), we have

$$v(x) = Ee^{-rT} v(X^*(T) + cE\int_0^{T_n} e^{-rt} d\xi_t^* + E\int_0^{T_n} e^{-rt} X^*(t)dt \tag{2.25}$$

Letting $T \to \infty$ in (2.25) and using the property $E\lim_{T\to\infty} e^{-rT} v(X^*(T)) = 0$, we obtain

$$v(x) = cE\int_0^{\infty} e^{-rt} d\xi_t^* + E\int_0^{\infty} e^{-rt} X^*(t)dt \tag{2.26}$$

Combining (2.16), (2.24) and (2.26), we complete the proof.

An Explicit Solution

Theorem 2.1 has given a sufficient criterion for optimal objective function. Usually, it is quite difficult to find an explicit solution satisfying all the conditions for general parameters. However, under certain simplifications we can find an explicit form. Throughout this section, we assume that:

$$c > \frac{1}{r}, \quad \sigma < \frac{\mu}{rc-1}\sqrt{2\lambda c^2 + 2c} \tag{3.1}$$

Lemma 3.1 Let function $f(x)$ be

$$f(x)=\frac{1}{\theta_1 e^{\theta_1 x}(\theta_1-\theta_2)}\left[\theta_\lambda\frac{rc-1}{r+\lambda}-\theta_2(c-\frac{1}{r})\right]+\frac{1}{\theta_2 e^{\theta_2 x}(\theta_2-\theta_1)}\left[\theta_\lambda\frac{rc-1}{r+\lambda}-\theta_1(c-\frac{1}{r})\right]+\frac{\mu}{r^2}, \quad (3.2)$$

where $\theta_1 > 0 > \theta_2$ are the roots of $\frac{\sigma^2}{2}\theta^2+\mu\theta-r=0$, and $\theta_\lambda < 0$ is the negative root of $\frac{\sigma^2}{2}\theta^2+\mu\theta-(r+\lambda)=0$. Then there exists a unique constant m > 0 such that f(m) = 0; i.e.,

$$f(m)=\frac{1}{\theta_1 e^{\theta_1 m}(\theta_1-\theta_2)}\left[\theta_\lambda\frac{rc-1}{r+\lambda}-\theta_2(c-\frac{1}{r})\right]+\frac{1}{\theta_2 e^{\theta_2 m}(\theta_2-\theta_1)}\left[\theta_\lambda\frac{rc-1}{r+\lambda}-\theta_1(c-\frac{1}{r})\right]+\frac{\mu}{r^2}=0. \quad (3.3)$$

Proof. By simple differentiation, we see that

$$f'(x)=\frac{\theta_\lambda}{(\theta_1-\theta_2)}.\frac{rc-1}{r+\lambda}(e^{-\theta_2 x}-e^{-\theta_1 x})+\frac{c-\frac{1}{r}}{\theta_2-\theta_1}(\theta_2 e^{-\theta_1 x}-\theta_1 e^{-\theta_2 x}) . \quad (3.4)$$

From $\theta_\lambda < 0$, $\theta_1 - \theta_2 > 0$, c > $\frac{1}{r}$, $\theta_2 < 0 < \theta_1$, we have $f'(x) \le 0$. Using (3.1), we obtain

$$f(0)=-\frac{\theta_\lambda}{\theta_1\theta_2}.\frac{rc-1}{r+\lambda}+(c-\frac{1}{r}).\frac{\theta_1+\theta_2}{\theta_1\theta_2}+\frac{\mu}{r^2}$$

Using $\theta_1+\theta_2=\frac{-2\mu}{\sigma^2}$, $\theta_1\theta_2=\frac{-2r}{\sigma^2}$ and $\theta_\lambda=\frac{-\mu-\sqrt{\mu^2+2\sigma^2(r+\lambda)}}{\sigma^2}$, we can simplify $f(0)$ to

$$f(0)=\frac{-\mu-\sqrt{\mu^2+2\sigma^2(r+\lambda)}}{2r}.\frac{rc-1}{r+\lambda}+\frac{\mu c}{r}$$

which can be shown that f(0) > 0 under the assumption (3.1).

Since $\theta_1 > 0$, we have $\lim_{x\to\infty} e^{\theta_1 x}=\infty$. Then from the definition of $f(x)$, we obtain

$$\lim_{x\to\infty} f(x)=\lim_{x\to\infty}\left\{\frac{1}{\theta_2 e^{\theta_2 x}(\theta_2-\theta_1)}\left[\theta_\lambda\frac{rc-1}{r+\lambda}-\theta_1(c-\frac{1}{r})\right]+\frac{\mu}{r^2}\right\}=-\infty$$

where we used the facts that $\theta_1 > 0$, $\theta_2 < 0$, $\theta_\lambda < 0$, $\theta_2 - \theta_1 < 0$, and the condition (3.1).

Hence, there exists a unique $m \in (0,\infty)$ such that $f(m) = 0$; which concludes the proof.

Lemma 3.2 For the constant m given by (3.3), there exits a function $\hat{v}(x)$ satisfying the following:

$$\frac{\sigma^2}{2}\hat{v}''(x)+\mu\hat{v}'(x)-(r+\lambda)\hat{v}(x)+x+\lambda(\hat{v}(m)+c(x-m))=0, \quad \forall x\in(0,\infty), \quad (3.5)$$

$$\hat{v}''(x)\le 0, \quad \forall x\in(0,\infty),$$
$$\hat{v}'(m)=c. \quad (3.6)$$

Proof. For simplicity, we denote

$$\hat{v}'(x)=B_1 e^{\theta_\lambda x}+B_2 x+B_3, \quad (3.7)$$

where

$$B_1=\frac{1}{\theta_\lambda e^{\theta_\lambda m}}\frac{rc-1}{r+\lambda}<0, \qquad B_2=\frac{1+\lambda c}{r+\lambda},$$
$$B_3=\frac{1}{r+\lambda}\left\{\frac{\mu(1+\lambda c)}{r+\lambda}+\lambda\left[\frac{1}{\theta_\lambda}(c-\frac{1}{r})+\frac{m}{r}+\frac{\mu(1+\lambda c)}{r(r+\lambda)}-cm\right]\right\} \quad (3.8)$$

From (3.7), we have

$$\hat{v}'(x)=B_1\theta_\lambda e^{\theta_\lambda x}+B_2, \qquad \hat{v}''(x)=B_1\theta_\lambda^2 e^{\theta_\lambda x},$$

using which and Eq.(3.3), we can see that B_2x+B_3 is a particular solution to (3.5), and $e^{\theta_\lambda x}$ is a general solution to the corresponding homogeneous equation:

$$\frac{\sigma^2}{2}\hat{v}''(x)+\mu\hat{v}'(x)-(r+\lambda)\hat{v}(x)=0.$$

Thus, (3.5) follows. The rest proof can be done by simple algebraic computations.

Theorem 3.1 Denote function $w(x)$ by

$$w(x)=\begin{cases} A_1e^{\theta_1 x}+A_2e^{\theta_2 x}+A_3x+A_4, & 0\le x\le m \\ \hat{v}(x) & \forall x\ge m \end{cases} \tag{3.9}$$

where $\hat{v}(x)$ is given by (3.7) and

$$\begin{aligned} A_1&=\frac{1}{\theta_1e^{\theta_1 m}(\theta_1-\theta_2)}\left[\theta_\lambda\frac{rc-1}{r+\lambda}-\theta_2(c-\frac{1}{r})\right],\\ A_2&=\frac{1}{\theta_2e^{\theta_2 m}(\theta_2-\theta_1)}\left[\theta_\lambda\frac{rc-1}{r+\lambda}-\theta_1(c-\frac{1}{r})\right],\qquad A_3=\frac{1}{r},\qquad A_4=\frac{\mu}{r^2}\end{aligned} \tag{3.10}$$

Then $w(x)$ satisfies all the conditions of Theorem 2.1. Consequently, it is the optimal objective function of Problem 1.1, and its corresponding optimal control ξ^* is given by (2.17).

Proof. Note that $w(x)=A_1e^{\theta_1 x}+A_2e^{\theta_2 x}+A_3x+A_4$ is the solution to the following equation

$$\frac{\sigma^2}{2}w''(x)+\mu w'(x)-rw(x)+x=0.$$

From (3.7) and (3.8), $\theta_1+\theta_2=\frac{-2\mu}{\sigma^2}$, $\theta_1\theta_2=\frac{-2r}{\sigma^2}$, $\theta_\lambda=\frac{-\mu-\sqrt{\mu^2+2\sigma^2(r+\lambda)}}{\sigma^2}$, after some lengthy algebraic calculations, we have

$$\hat{v}(m)=B_1e^{\theta_\lambda m}+B_2m+B_3=\frac{\mu(rc+2\lambda c+1)}{2r(r+\lambda)}-\frac{(rc-1)\sqrt{\mu^2+2\sigma^2(r+\lambda)}}{2r(r+\lambda)}+\frac{m}{r}.$$

From (3.9) and (3.10), we have

$$\begin{aligned} w(m)&=A_1e^{\theta_1 m}+A_2e^{\theta_2 m}+A_3m+A_4\\ &=\frac{\mu(rc+2\lambda c+1)}{2r(r+\lambda)}-\frac{(rc-1)\sqrt{\mu^2+2\sigma^2(r+\lambda)}}{2r(r+\lambda)}+\frac{m}{r}.\end{aligned}$$

Hence $w(x)$ is continuous at point m, which shows that $w(x)\in C([0,\infty))$.

From (3.9), we know that

$$w'_-(m)=c=\hat{v}'(m)=w'_+(m).$$

Hence

$$w(x)\in C^1([0,\infty))$$

The boundness and positive characterization of $w'(x)$ follow immediately from Lemmas 3.1 and 3.2 and (3.10).

From (3.7)-(3.10), we see that $\hat{v}''(m)=B_1\theta_\lambda^2e^{\theta_\lambda m}=\theta_\lambda\frac{rc-1}{r+\lambda}$. On the other hand, from (3.9), we have

$$w''(m)=\theta_1^2A_1e^{\theta_1 m}+\theta_2^2A_2e^{\theta_2 m}=\theta_\lambda\frac{rc-1}{r+\lambda},$$

from which we have $w''(m)=\hat{v}''(m)$, hence $w(x)\in C^2([0,\infty))$.

From (3.2), (3.9) and (3.10), we know $w(0)=A_1+A_2+A_4=0$, hence condition (2.4) follows.

When $x>m$, $w''(x)=B_1\theta_\lambda^2e^{\theta_\lambda x}\le 0$, $w'(m)=c$, from (3.8),

$\lim_{x\to\infty}w'(x)=\lim_{x\to\infty}e^{\theta_\lambda(x-m)}\frac{rc-1}{r+\lambda}+\frac{1+\lambda c}{r+\lambda}=\frac{1+\lambda c}{r+\lambda}>0$, so we have (2.5).

From (3.1) and (3.10), we have $A_1 > 0$, $A_2 < 0$, and when $x \in [0, m]$,

$w''(x) = \theta_1^2 A_1 e^{\theta_1 x} + \theta_2^2 A_1 e^{\theta_2 x} \le \theta_1^2 A_1 e^{\theta_1 m} + \theta_2^2 A_1 e^{\theta_2 m}$. From (3.10), we have

$\theta_1^2 A_1 e^{\theta_1 m} + \theta_2^2 A_1 e^{\theta_2 m} = \theta_\lambda \dfrac{rc-1}{r+\lambda} \le 0, 0$, hence condition (2.1) holds.

From Lemma 2.1, we know that (2.6) holds. By (3.9) we know that $v(x)$ satisfies conditions (2.2), (2.8), and (2.9).

So far, we have shown that $w(x)$ satisfies all the conditions of Theorem 2.1. Hence $w(x)$ is the optimal objective function, and its corresponding optimal control is ξ^* , which completes the proof of Theorem 3.1.

Note that the state process and the object structure in this model is not that complicated, but we can generalize them without too much difficult. For example, we can generalize our results to a model with the following state process and objective structure:

$$X_t = x + \int_0^t \mu(X_s)ds + \int_0^t \sigma(X_s)dW_s + \xi_t, \quad t \ge 0 \tag{4.1}$$

$$v(x) = E\int_0^{\tau_0} e^{-rt}\{g(X_t)d\xi_t + h(X_t)dt\}$$

where $\mu(x)$, $\sigma(x)$, g(x) and $h(x)$ are more general functions. In that case, we can find an optimal control $\xi^* \in \Pi$ such that $V_{\xi^*} = \sup_{\varsigma \in \Pi} V_\xi(x)$. The details will be presented in our future work.

References

[1] N. Ikeda, S.Watanabe, Stochastic Differential Equations and Diffusions Process, North-Holland, 1989.

[2] V.E.Benes, L.A. Shepp, H.S. Witsenhausen, Some solvable stochastic control problems, Stochastics 4 (1980) 39-83.

[3] L. Alvarez, L. Shepp, Optimal harvesting of stochastically fluctuating populations, J. Math. Biol. 37 (1997) 155-177.

[4] J.A. Baiter, H. Chernoff, Sequential decisions in the control of a spaceship, In: L.M. Le Cam and J. Neyman (Eds.), Prob. 5th Berkely Symp. Math Statist Prob., Vol.3, University of California Press, Berkely, 1966, pp.181-207.

[5] A.K. Dixii, R.S. Pindyck, Investment Under Uncertainty, Princeton University Press, 1994.

[6] W.H. Fleming, H.M. Soner, Controlled Markov Processes and Viscosity Solutions, Springer, New York, 1993.

[7] J.M. Harrison, M.I. Taksar, Instantaneous control of Brownian motion, Math Operat. Res. 8 (1983) 439-453.

[8] I. Karaizas, A class of singular stochastic control problems, Adv. Appl. Prob. 15 (1983) 225-254.

[9] E.M. Lungu, B. Ksendal, Optimal harvesting from a population in a stochastic crowded environment, Math. Biosci. 145 (1997) 47-75.

[10] S.E. Sherve, J.P. Lehoczky, D.P. Gavers, Optimal consumption for general diffusions with absorbing and reflecting barriers, SIAM J. Control Optim. 22 (1984) 55-75.

[11] K. Liu, M. Qin, C. Lu, On sufficient and necessary of existence for a class of singular optimal stochastic control. Journal of Systems Science and Complexity 16 (2003) 424-437.

[12] K. Liu, M. Qin, C. Lu, A class of Stationary models of singular stochastic control, Mathematica Acta Scientia 24B(1) (2004) 139-150.

[13] A. Weerasinghe, A bounded variation control problem for diffusion processes, SIAM J Control Optim. 44 (2005) 389-417.

[14] A. Bensoussan, J.-L. Lions, Impulse Control and Quasi-Variational Inequalities, Gauthier-Villars, Paris, 1984.

[15] J.M. Harrison, T.M. Sellke, A.J. Taylor, Impulse control of Brownian motion, Math. Operat. Res. 8 (1983) 454-466.
[16] J.L. Menaldi, M. Robin, On some cheap control problems for diffusion process, Trans. Amer. Math. Soc. 278 (1983) 771-802.
[17] K. Liu, M. Qin, C. Lu, A class of stationary impulse stochastic control with state of semimartingal (I), J. Sys. Sci. Math. Scis. 25 (2005) 96-105.
[18] K. Liu, M. Qin, C. Lu, A class of stationary impulse stochastic control with state of semimartingal (II), J. Sys. Sci. Math. Scis. 25 (2005) 237-248.
[19] W. Hui, Some control problems with random intervention times, Adv. Appl. Prob. 33 (2001) 404-422.
[20] F.C. Klebaner, Introduction to Stochastic Calculus with Applications, World Scientific Publishing Company, Beijing, 1999.
[21] I. Karatzas, S.E. Shreve, Brownian Motion and Stochastic Calculus, Springer Verlag, New York, 1988.
[22] P. Bremaud, Point Processes and Queues: Martingal Dynamics, Springer, New York, 1981.
[23] L.C.G. Rogers, D. Williams, Diffusions Markov Processes and Martingals: Vol.1. Foundations, Cambridge University Press, New York, 2000.

Advanced Materials Research Vols. 450-451 (2012) pp 56-59

doi:10.4028/www.scientific.net/AMR.450-451.56

Study on compressive strength and flexural properties of igneous fiber hydraulic concrete

Jiandong Wang[1, a], Huating Liu [1,b], Junzhi Zhang[1,c] and Lingjie Wu[1,d]

[1]College of Civil Engineering and Architecture, Zhejiang University of Technology, Hangzhou, Zhejiang 310014, P.R. China

[a]wjd@zjut.edu.cn, [b]lhting1985@sina.com, [c]jzzhang@zjut.edu.cn, [d]79186643@qq.com

Keywords: basalt fiber, carbon fiber, concrete, compressive strength, flexural strength

Abstract. This study investigates the compressive strength, flexural strength and flexural modulus of the short-chopped igneous fiber reinforced concrete, short-chopped carbon fiber reinforced concrete and plain concrete. Experimental results show that both short-chopped igneous fiber and carbon fiber can improve the compressive strength and flexural behavior of the concrete significantly, and the reinforcing effectiveness of igneous fiber is better that of carbon fiber.

Introduction

Igneous fiber and carbon fiber is a new material of 21st century. Both have outstanding mechanical properties, such as high temperature resistance, corrosion resistance, etc., and widely used all walks of life [1,2]. The main components of igneous fiber is basalt, and so they were sometimes called basalt fiber.

Concrete compressive strength and flexural performance was the main content of reinforced concrete structural design and construction quality control [3]. In this paper the compressive strength, flexural strength and flexural modulus of the short-chopped igneous fiber reinforced concrete, short-chopped carbon fiber reinforced concrete and plain concrete are tested, the corresponding law was also analyzed.

Experimental

Raw Materials. The cement of experimental concrete is a kind of 42.5 composite Portland cement. The fine aggregate is a kind of river sand of 2.5 fineness modulus, and the maximum gravel diameter of coarse aggregate is 40 mm. Mixing and curing water are the local city water.

The short-chopped igneous fiber used in this experiment is a kind of commercial continuous basalt fiber from Hengdian Group Shanghai E'Jin Basalt Fiber Co., Ltd, and the diameter of the single wire of fiber is 10.43 μm, and the mean tensile strength of the single wire of fiber is 416.8 MPa. And there are differences in the production engineering with different basalts fiber origin [4].

The used short-chopped carbon fiber in this check experiment is also commercial PAN-based carbon fiber from Nanjing WeiDa composite material Co., Ltd., the diameter of the single wire of fiber is 7 μm, the density is 1.76 g/m3, the elastic modulus is 200 GPa the tensile strength is 3.6 GPa, and the rupture extensibility is 1.5 %.

Mix Proportion of Test Concrete. Three types of concrete were designed, plain concrete(C), igneous fiber reinforced concrete (BF) and carbon fiber reinforced concrete (CF), with two water-cement ratio(w/c), five volume dosage (0.1 %, 0.3 %, 0.5 %, 0.7 % and 0.9 % volume ratio of cement) and three short-chopped fiber length (10 mm, 15 mm and 20 mm). The mix proportion of concrete samples of each water-cement is listed in the Table 1.

Table 1 Mix proportion of experimental concrete[kg.m^{-3}]

No.	cement	water	sand	stone	w/c
1	380	190	578	1229	0.50
2	317	190	597	1269	0.60

Testing Methods and Results

Testing Methods. The compression test and bending test for the test samples conform to the Chinese Code [5]. Dimension of compression specimen is 150 mm × 150 mm × 150 mm, and 100 mm × 100 mm × 400 mm of bending specimen. The specimen quantity of each specification concrete including different mix proportion and different fiber and different mix quality of fiber is three samples, and all the samples are formed at the same time.

In the production process of fiber concrete specimens, the feed sequence, mixing method, mixing time have an impact on its performance [6]. Using compulsion type concrete mixer is capable of producing a good uniformity and quality for concrete mixture. Feeding order as follows: add materials other than fiber during the first stirring, and then gradually into fibers, stir 3 ~ 5 min when all the fiber input.

Results and Discussion

Test Results. Compressive strength and flexural behavior of three types of concrete is very obvious, and the concrete details can obtained from Figure 1, Table 2 and Table 3 [7]. The mean compressing strength of three check plain concrete specimens in water-cement 0.50 is 25.01 MPa, mean flexural strength is 4.08 MPa, and mean flexural modulus is 32.85 Gpa, while 21.74 MPa, 3.43 MPa, 32.2 GPa respectively when the water-cement ratio of experimental plain concrete is 0.60.

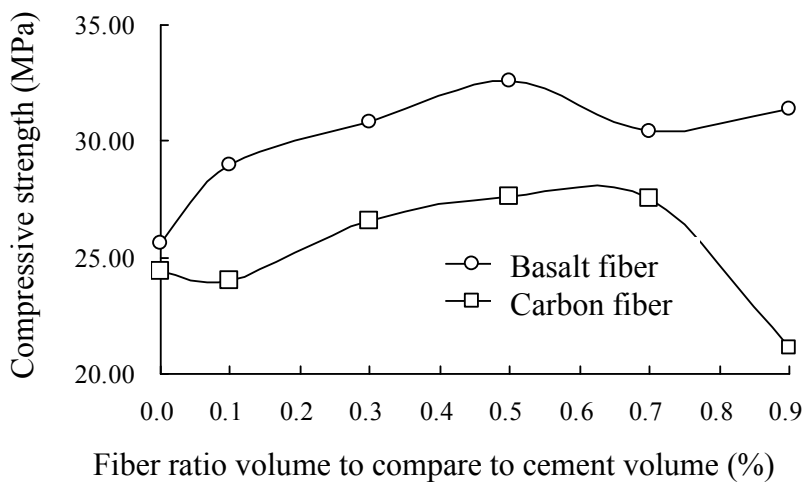

Fig.1 Compressive strength of fiber concrete with the ratio volume to compare to cement volume (w/c 0.50, fiber length 20 mm)

The mean compressing strength and flexural behavior of different fiber concrete of same water-cement and different fiber volume ratio to compare to cement volume is listed the Table2.

Table 2 is the mean compressive strength and flexural behavior of fiber concrete of same w/c and fiber length of different volume ratio to compare to cement volume.

Table 2 Cmpressive strength and flexural behavior of fiber concrete of 0.50 w/c and fiber length of 20 mm

Fiber type	Fiber ratio volume (%)	Compressive Strength (MPa)	Flexural Strength (MPa)	Flexural modulus (GPa)
BF	0.1	28.96	4.70	37.8
CF	0.1	24.04	3.67	31.6
BF	0.3	30.75	4.81	36.2
CF	0.3	26.61	4.01	31.9
BF	0.5	32.64	4.66	36.4
CF	0.5	27.63	4.19	31.1
BF	0.7	30.37	4.74	35.5
CF	0.7	27.52	3.91	28.9
BF	0.9	31.37	4.47	34.2
CF	0.9	21.16	3.55	29.1

Table 3 is the mean compressive strength and flexural behavior of fiber concrete of same fiber content and different fiber length and w/c.

Table 3 Compressive strength and flexural behavior of fiber concrete of different w/c and fiber length with 0.1%fiber ratio volume

Fiber type	w/c	Fiber Length (mm)	Compressive Strength (MPa)	Flexural Strength (MPa)	Flexural modulus (GPa)
BF	0.5	10	29.18	4.74	35.0
BF	0.6	10	23.74	4.24	33.1
CF	0.5	10	26.27	3.86	35.8
CF	0.6	10	21.45	3.33	32.2
BF	0.5	15	29.05	4.97	37.0
BF	0.6	15	20.38	3.33	31.1
CF	0.5	15	24.16	3.75	30.8
CF	0.6	15	22.22	3.47	38.7
BF	0.5	20	28.96	4.70	37.8
BF	0.6	20	18.80	3.32	30.1
CF	0.5	20	24.04	3.67	31.6
CF	0.6	20	25.34	3.88	32.4

Discussion.

1) Admixture of short-chopped fiber can reinforce the concrete compressive strength. Admixture of igneous fiber and carbon fiber can increase the maximum compressive strength of ordinary concrete up to 27.3 % and 13.1 %, respectively.

2) Mixing of short-chopped fibers can improve the concrete flexural strength. For example, when the water-cement ratio concrete is 0.50, mean flexural strength of igneous fiber reinforced concrete is 8.7 % higher than that of plain concrete, and the mean flexural strength of carbon fiber reinforced concrete increase of 4.3 %.

3) It can be drawn from 1) and 2) that the reinforcing effectiveness of concrete mix with short-chopped igneous fiber is better than that of carbon fiber.

4) The compressive strength of fiber concrete increases with the increase of short-chopped fiber content first, and then decrease after reach the optimum content of fiber. When fiber content from 0.1 % to 0.5 %, the compressive strength increased with the dosage, but in 0.7 % to 0.9 %, the compressive strength decreased.

Conclusion

1) Compared with plain concrete, the short-chopped basalt fiber and carbon fiber can all enhance compressive strength and flexural properties of hydraulic concrete. Maximum compressive strength of concrete mix with igneous fiber and carbon fiber can increase by 27.3 % and 13.1 % respectively, and there exist the optimum volume ratio of fiber to compare to cement volume.

2) The reinforcing effectiveness of concrete mix with short-chopped igneous fiber is better than that of carbon fiber.

Acknowledgements

This work was financially supported by the Science and Technology Plan Project of the Ministry of Water Resources of P. R. China No. 200901065.

References

[1] F.J. Qi, J.W. Li and C.X. Li, et al.: Hi-Tech Fiber & Application. Vol.31(2), 42-46(2006). (in Chinese)
[2] J.F. Mao, W.G. Dong, and S.Z. Cong, et al.: Technical Textiles. (10), 38-40(2007). (in Chinese)
[3] Z.X. Wu, in: Research on Basic Mechanical Properties and Application of Basalt Fiber Reinforced Concrete [D]. *MD thesis*, Wuhan University of Technology, Wuhan (2009). (in Chinese)
[4] G.L. Huang, Z.J. Sun, and M.C. Wang, et al.: Fiber Reinforced Plastics/Composites. (1), 24-27(2006). (in Chinese)
[5] G.X. Chen, Y.B. Cai, et al.: Test Code for Hydraulic Concrete [S]. Industry Standard of the People's Republic of China(SL352-2006): Beijing: China WaterPower Press, 2006.
[6] Z.X Wu, H.Q Yuan, Z.A Lu, et al.: Concrete. (9), 67-68(2009). (in Chinese)
[7] H.T. Liu, in: Experimental Study on the Basic Property of Chopped Basalt Fiber Hydraulic Concrete and Mortar [D]. *MD thesis*, Zhejiang University of Technology, Hangzhou(2011). (in Chinese)

Advanced Materials Research Vols. 450-451 (2012) pp 60-63

doi:10.4028/www.scientific.net/AMR.450-451.60

Study on adsorption of Methylene Blue by the Modified Kaolin

Muqing Qiu[1, a], Jiajia Zhang[1, b] and Jiawei Ni[1, c]

College of Life Science, Shaoxing University, Zhejiang Shaoxing, P.R. China, 312000

[a]qiumuqing@126.com, [b]jiajiazhang@126.com, [c]jiaweini@126.com

Keywords: Zeolite；Composite Photocatalyst；Methylene Blue；Modified Kaolin

Abstract. Using Kaolin as the main raw material,l ultrafine particles modified Kaolin were prepared. Then loading transition metals (copper and zinc), the final modified Kaolin composite photocatalyst was finished. This study used a composite photocatalyst in three main factors photocatalytic oxidation degradation of methylene blue simulated waste Textile Industry water effects. The results showed that the best conditions for simulated wastewater of 100 mL was: methylene blue initial concentration of 40 mg/L, hydrogen peroxide of 0.4 mL, composite photocatalyst of 60 mg, pH 10.21. Under this condition, the chromaticity of methylene blue dropped from 1 600 to 10 after aeration reaction of 120 min, and its removal rate was 99.32%.

Introduction

The research of the transition metal catalyst taking TiO_2 as the representative has been studied extensively, which fully demonstrates potential and profound application background of the heterogeneous photocatalytic technology in the production of clean energy and environmental pollution. However, its application is limited as the result of the high expense of titanium compounds. And kaolin modified composite photocatalyst solves the problem to some extent, which are ultrafine particles prepared with a large number of cheap, non-toxic and pollution-free kaolin as the main raw material. Through ion exchange and transition metal support, kaolin modified is finally changed to kaolin modified composite photocatalyst. With water soluble azo dyes for representative compounds – methylene blue as the research object, and through the experiment of the composite photocatalyst for photocatalysis degradation, we study certain factors which may influence the methylene blue degradation, including initial concentration of methylene blue , hydrogen peroxide dosage, composite photocatalyst dosage, etc, on the purpose of providing reference to the wastewater treatment in textile dyeing industry.

Materials and Methods

Reagent

A simulated dye wastewater with a certain concentration of methylene blue solution of reserve. 30% (mass fraction, similarly hereinafter) hydrogen peroxide. Concentrated sulfuric acid. sodium hydroxide. aluminum sulfate. ammonium chloride. zinc sulfate. copper sulfate. methylene blue (above for the analysis of pure). kaolin (chemical). Silica sol, etc.

Instrument

The main instruments include type of UV-1200 UV-Vis spectrophotometer, UV1102 type ultraviolet visible spectrophotometer, 101-2 type drying box, SXL-1304 type programmable box-type electric furnace, AUY220 analytical balance, ultraviolet disinfection lamp (20 W), incandescent lamp (40 W), DF-101S (T) heat collection type constant temperature magnetic stirrer, 79-1 type magnetic heating stirrer, JJ-3C six electric mixer, air compressor, PHS-3C type precision pH, ADL-6C type centrifuge, CTL-2 type centrifuge chemical oxygen demand meter, SHB-B type SHB-B multi-usage vacuum pump with water circulation.

Kaolin Nano Molecular Sieve Preparation

Firstly, weigh appropriate amount of sodium hydroxide and aluminum sulfate, dissolve them in deionized water, instillate silica sol under high speed magnetic stirring, then mix into a transparent colloid, Finally, Na_2O: Al_2O_3: SiO_2: H_2O=16:1:16: 210 (mole ratio), age for 48h under room temperature as a directing agent.

Secondly, under 750℃ for 2h kaolin can be changed into metakaolin with active Al and Si; weigh sodium hydroxide and dissolve them in certain deionized water, add metakaolin and stir evenly, drip add silica sol in drops under magnetic high speed stirring; then add the directing agent so that Na_2O: Al_2O_3: SiO_2: H_2O: directing agent=7.8: 1: 16: 400: 0.1(mole ratio); seal glass under 725 r/min magnetic stirring (to prevent water evaporation) crystallization for 5.5h 90℃ water bath; while it is hot add saturated solution of ammonium chloride to the reaction liquid with crystal precipitation (to promote filter), suck with vacuum pump, wash with deionized water to neutral, dry for 12h under 120℃, finally after calcinations under 600℃ for 2h, crush and sieve to get ultrafine particles kaolin modified.

Load of Transition Metal Ion

Take 1 g nano molecular sieve as carrier, and add 1.9789 g zinc sulfate and 1.7681 g copper sulfate crystals with a 500 mL mixture, with the closure to prevent the evaporation of moisture, and filter suspensions after magnetic stirring at 725 r/min for 24h at room temperature, and wash by deionized water to neutral, bake under 120℃ for 12h, roast at 500℃ for 3h ,then we get kaolin modified composite photocatalyst.

Mechanism of Methylene Blue Decolorization

Methylene blue (shortened form MB), molecular formula: $C_{16}H_8N_3SCl{\cdot}3H_2O$, is a kind of sulfur and nitrogen benzene chromogenic agent, its structure type is similar to anthracene, it is difficult to oxidize it by potassium dichromate, and we cannot determine its concentration accurately according to COD ; but at low concentrations, there is a very good linear relationship between MB absorbance and concentration， which is in accordance with the Lambert-Beer Law, so we can use the maximum absorption wavelength absorbance to reflect its concentration at. The molecule of MB is shown in Fig.1. As shown in Fig.1, the the sulfhydryl (-S-) is the main color group, because it is an electron-withdrawing group, the electron density of which is relatively large, and when it reacts with the composite photocatalyst, it will be oxidized, and the absorbance of the group was less than 180 nm, so MB will fade after oxidation.

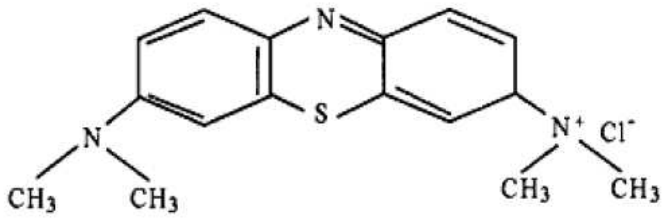

Fig.1 The molecule of MB

Experimental Method

Add 100 mL MB wastewater in a 500 mL beaker, adjust pH in the solution to 10.21, and aetate for 120 min under irradiation of 20W ultraviolet disinfection lamp. Take the supernatant and centrifuge it to determination its absorbance. Examines the initial concentration of MB, dosage of 30% hydrogen peroxide and the effect composite photocatalyst dosage taking on the degradation rate of MB. Calculate the degradation of MB according to the following formula:

$$\omega = (1 - A / A_0) \times 100\% \quad (1)$$

Formula: ω for the degradation rate of MB, %; A_0 for the solution absorbance before the reaction; A for the solution absorbency after the reaction.

Maximal Absorption Wavelength of Methylene Blue Determination

After the preparation of a certain concentration of MB solution, scan the spectrum of MB solution absorbance in the range of 400 to 800 nm (including the visible light range), at the scanning interval of 0.5 nm and at the scanning speed of 100nm/min. The result of the determination at different wavelength absorbance of MB solution is shown in Fig.2, and the maximum absorbance wavelength is 655.0 nm..

Results and Discussion

The Effect of MB Initial Concentration on Photocatalytic Degradation of MB

Shown by Figure 3, the lower of MB solution concentration is, the higher the rate of degradation. When the initial concentration is 40 mg/L, degradation rate of MB reach 40.32%; and when it is increased to 640 mg/L, the degradation is only 5.21%. As a result, 40 mg/L is chosen as the initial concentration of the following experiments.

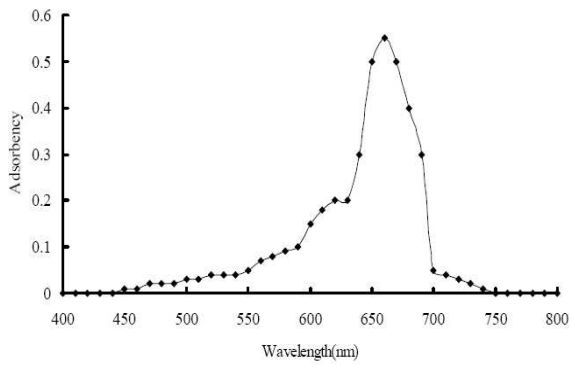

Fig.2 The Maximal adsorbency of MB at the different wavelength

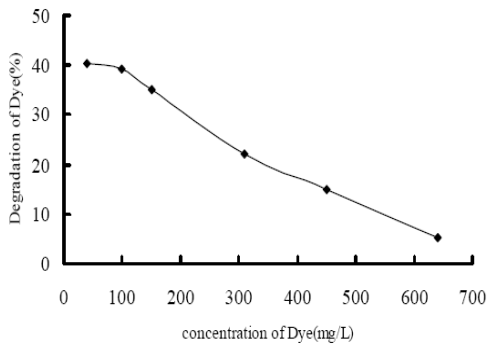

Fig. 3 Effect of MB initial concentration on photo-degradation

Effect of Hydrogen Peroxide Dosage on Photocatalytic Degradation

From Figure 4, it is known that a small amount of hydrogen peroxide have a very significant role on the degradation of MB. With the increasing of hydrogen peroxide dosage, the degradation rate of MB decreases. It is because when the concentration of hydrogen peroxide is low, the generation of free radical •OH increases with the hydrogen peroxide concentration， the MB degradation rate are relatively high in result. When the concentration of hydrogen peroxide is high, the excess hydrogen peroxide is a free radical scavenger, consuming •OH free radical and reducing the utilization rate of •OH free radical. The reaction type is: $\bullet OH + H_2O_2 \rightarrow H_2O + HO_2\bullet$. When hydrogen peroxide is excessive, owing to the large number of $HO_2\bullet$ free radical with a large quantity of oxygen generated by photolysis promoting the removal of MB, the MB degradation rate is slowly rising again. . Considering the cost of wastewater treatment by both treatment effect, determine the following experimental hydrogen peroxide dose selection for 0.4 mL. . Considering both the cost of wastewater treatment and treatment effect, 0.4mL is chosen as the hydrogen peroxide dosage in the following experiment.

Effect of Photocatalyst Dosage on Degradation

The effect of Photocatalyst dosage on degradation is shown in Figure 5. Figure 5 shows, the increase of composite photocatalyst dosage in solution and metal containing optical active promote the degradation of MB solution. And the maximum MB degradation rate is reached on condition when composite photocatalyst dosage is 60 mg. With the continuing increasing of the photocatalyst concentration, excessive composite photocatalyst has hindered the solution on the absorption of light, thus the MB degradation rate decrease. As a result, 60 mg is chosen as the composite photocatalyst dosage in the experiment.